

Transient and Equilibrium Synchronization in Complex Neuronal Networks

Luciano da Fontoura Costa

*Institute of Physics at São Carlos, University of São Paulo,
PO Box 369, São Carlos, São Paulo, 13560-970 Brazil*

(Dated: 16th Jan 2008)

Transient and equilibrium synchronizations in complex neuronal networks as a consequence of dynamics induced by having sources placed at specific neurons are investigated. The basic integrate-and-fire neuron is adopted, and the dynamics is estimated computationally so as to obtain the activation at each node along each instant of time. In the transient case, the dynamics is implemented so as to conserve the total activation entering the system. In our equilibrium investigations, the internally stored activation is limited to the value of the respective threshold. The synchronization of the activation of the network is then quantified in terms of its normalized entropy. The equilibrium investigations involve the application of a number of complementary characterization methods, including spectra and Principal Component Analysis, as well as of an equivalent model capable of reproducing both the transient and equilibrium dynamics. The potential of such concepts and measurements is explored with respect to several theoretical models, as well as for the neuronal network of *C. elegans*. A series of interesting results are obtained and discussed, including the fact that all models led to a transient period of synchronization, whose specific features depend on the topological structures of the networks. The investigations of the equilibrium dynamics revealed a series of remarkable insights, including the relationship between spiking oscillations and the hierarchical structure of the networks and the identification of twin correlation patterns between node degree and total activation, implying that hubs of connectivity are also hubs of integrate-and-fire activation.

PACS numbers: 05.10.-a, 05.40Fb, 89.70.Hj, 89.75.k

‘Measure what is measurable, and make measurable what is not so.’ (G. Galilei)

I. INTRODUCTION

Few research areas have received so much attention as neuronal networks and complex networks. Investigations at the intersection of these two areas are particularly promising because they naturally integrate the emphasis on structure typical of complex networks and the dynamics systems features of neuronal networks. Such a multidisciplinary area is henceforth called *complex neuronal networks*. Despite the many possibilities for cross-fertilization between these two areas, relatively few related works have been reported. Probably the first investigations in neuronal complex networks were reported in [1, 2]. Other related works include [3, 4, 5]. Another issue of special interest regarding the dynamics of systems underlain by complex connectivity regards their synchronization. Synchronization plays an important role in several natural situations, including heartbeats and overall brain activity. Several works addressing synchronization in complex networks have been reported in the literature (e.g. [6, 7, 8, 9, 10, 11, 12, 13, 14, 15, 16, 17, 18, 19, 20, 21]). The investigation of synchronization in neuroscience and neuronal networks has a long history (e.g. [22, 23, 24, 25]). More recently, growing attention has been placed on synchronization of complex neuronal networks (e.g. [26, 27, 28, 29]). However, a great deal of such investigations has had their attention concentrated on models of individual neuronal activation

(e.g. Hodgkin-Huxley or Kuramoto) which are more sophisticated than the integrate-and-fire individual neuron model. Though many interesting results have been produced by such works, it is felt that a more systematic exploration of the relationship between synchronization and the different types of topologies in complex networks can be achieved by using simpler models for the neuronal dynamics, such as the integrate-and-fire approach, which allows faster computational simulations

The current article addresses the study of synchronization during the transient activation of complex networks with different topological features involving neurons of the integrate-and-fire type under conservation of the incoming activity. Although intrinsically related to neuronal networks, such results extend immediately to other types of systems involving integration-and-fire dynamics, especially production systems in which the output of a node requires the integration of specific inputs in order to yield a product (e.g. production of molecules, industrial production, or computational calculations in parallel systems). In this respect, the delay implemented by the combination of the integrator and non-linear element would act as a mechanism for favoring the chances of receiving all required inputs before the node can act on them.

Specific nodes are chosen as source of activation, and their effect in activating other neurons is sound and objectively quantified in terms of the instantaneous synchronization, a measurement defined in terms of the normalized entropy of the node activations at a given instant of time. The normalized instantaneous synchronization (NIS) is related to the entropy of the system

activation (e.g. [20, 30, 31]), but also takes into account the number of nodes already activated. Such an analysis of the overall synchronization of the network is performed with respect to 6 theoretical models of networks (Erdős-Rényi, Barabási-Albert, Watts-Strogatz, a geographical network, as well as two knitted networks). The neuronal network of *C. elegans* [6] is also investigated. The obtained results indicate that the overall synchronization tends to present a peak along the medium term, collapsing subsequently. In addition, each type of network implied specific features regarding the network activation and instantaneous synchronization.

The patterns of regular spiking arising at the equilibrium as a consequence of synchronization of the individual firings are also investigated by using a series of characterization methodologies as well as an equivalent model.

This article starts by summarizing the main concepts in complex networks and neuronal networks and proceeds by describing the normalized instantaneous synchronization concept, which is subsequently applied for the characterization of the synchronization in 6 networks of distinct kinds. The equilibrium investigations are reported subsequently with respect to Erdős-Rényi and Watts-Strogatz Networks.

II. BASIC CONCEPTS

This section summarizes the main concepts in network representation, measurement, random walks, as well as the six network models assumed in the present article.

A. Complex Networks Basics and Models

A weighted, directed network Γ can be fully represented in terms of its *weight matrix* W . Each edge extending from node i to node j , with associated weight v , implies $W(j, i) = v$. The absence of connection between nodes i and j implies $W(j, i) = 0$. The *out-degree* of a node i , henceforth expressed as k_{out} , corresponds to the number of outgoing edges of that node. The *out-strength* of a node i , s_{out} , is given by the sum of the respective weights of all outgoing edges. Similar definitions hold for the *in-degree* and *in-strength*.

Six models of complex networks are considered in the present article: Erdős-Rényi (ER), Barabási-Albert (BA), Watts-Strogatz (WS), a geographical model (GG) [32, 33, 34], as well as the path-regular network (PN) and path-transformed model (PA) [35, 36, 37, 38]. The ER network (see also related works by [39]) was grown by taking each possible edge with constant probability, the BA structure was grown by using the traditional preferential attachment scheme [32], and the WS was derived from a linear regular network with rewiring rate 0.1 [7, 8]. The geographical network (GG)

is obtained by distributing the nodes through a two-dimensional space and connecting all pairs of nodes which have distance smaller than a fixed threshold. The two knitted networks are the path-regular (PN) and path-transformed BA (PA) networks [36, 37]. Both these networks are formed by paths. The PN network is grown by incorporating paths involving all network nodes, being intensely regular regarding several of its topological features [37, 38]. The PA network can be obtained by transforming (from stars to paths) a BA network with the same number of nodes. All networks in this work have similar number of nodes and average degree. Only the largest connected component has been taken into account for each network. However, because of the relatively high average degree adopted in this work ($\langle k \rangle = 6$), most of the nodes end up belonging to the largest component.

B. Hierarchical Organization of Complex Networks

Given a complex network and a *reference node* i , its *hierarchical organization* can be obtained by flooding the network from the reference node [40]. The hierarchical organization includes the *concentric levels* (or hierarchical levels) of the network, namely the levels containing the nodes which are at successive shortest path distances from the reference node i . So, the first concentric level incorporates the original nodes which are at shortest path distance 1 from i (i.e. they are the immediate neighbors of i). The second concentric level includes the nodes which are at shortest path distance 2 from i , and so on. The connections between the reference node and the nodes at the h -level can be understood as implementing *virtual links* [41]. Once the hierarchical organization of a network has been obtained with respect to a specific node chosen as the reference, a series of measurements can be calculated [40, 42, 43, 44], including the *hierarchical number of nodes* $n_h(i)$, the *hierarchical degree* $k_h(i)$ and the *intra-ring degree* $a_h(i)$. The hierarchical number of nodes corresponds to the number of nodes within each respective concentric level. The hierarchical degree is equal to the number of edges from level h to level $h + 1$. The intra-ring (or intra-level) degree corresponds to the number of edges established within level h .

With the extension of the hierarchical organization to complex networks with asymmetric connections [45], the hierarchical degree needs to be split into *hierarchical indegree* and *hierarchical outdegree*. Therefore, the hierarchical indegree of level h with respect to node i , henceforth abbreviated as $ki_h(i)$, is equal to the number of edges received by level h from level $h - 1$. The hierarchical outdegree of level h is the number of edges sent from that level to level $h + 1$.

C. Instantaneous synchronization

Let Σ be a dynamic system implemented over a complex network involving N nodes. The activation of each node i at each time t is henceforth represented as $A(i, t)$. For simplicity, and without loss of generality, such activations can be normalized so that they become a statistical distribution. This can be done by defining the *probability of activation* of node i at time instant t to be $a(i, t) = A(i, t) / \sum_{i=1}^N A(i, t)$. The *entropy* of all such activations at t (e.g. [30, 31]) can not be immediately given as

$$\epsilon(t) = - \sum_{i=1}^N A(i, t) \log(A(i, t)) \quad (1)$$

Note that the maximum value of the entropy, corresponding to $\log(N)$, is achieved when all nodes have the same probability of activation $1/N$, i.e. the total activation is the most uniformly distributed amongst all the nodes.

Because the activation probability can be understood as a *mean frequency of activation* (e.g. [20]), it is interesting to consider the *instantaneous synchronization* of the system. A possibility is to use the following expression [20]

$$\sigma(t) = \frac{\log(N) - \epsilon(t)}{\log(N)} \quad (2)$$

Note that $0 \leq \sigma(t) \leq 1$, with the maximum entropy leading to null synchronization and minimal entropy leading to maximum synchronization. The nodes with null activation are not considered in the calculation of the entropy used for the synchronization because they are not really participating to the overall activation dynamics.

Though such a definition properly reflects the relationship between activation entropy and instantaneous synchronization, it does not take into account the fact that, especially during the transient period of time (but sometimes also at steady state), some nodes will not be active. Let us illustrate this problem through the following example. Let a dynamical system with $N = 100$ nodes have only 2 nodes activated at time t , e.g. because we are in the transient period and activation has not yet reached the other nodes. The probability activation therefore will be $a(t) = 0.5$, yielding $\epsilon(t) \approx 0.69$ and $\sigma = (\log(100) - \epsilon(t)) / \log(100) \approx 0.85$, indicating a high level of synchronization between the two nodes. Although this is really the case when only the two nodes are considered, the system actually involves other 98 nodes which are at zero activation. In order to better express the overall synchronization considering all the N nodes, we adopt henceforth the following alternative definition of the instantaneous synchronization of the dynamics:

$$\xi(t) = \frac{N_a}{N} \sigma(t) = \frac{N_a(t) \log(N) - \epsilon(t)}{N \log(N)} \quad (3)$$

where $N_a(t)$ is the number of nodes with non-zero activity at time t . Now, we will only have maximum synchronization $\xi(t) = 1$ when $N_a(t) = N$ and all nodes have the same activation probability. This measurement, henceforth called *normalized instantaneous synchronization* (NIS), is adopted throughout this work. Going back to the previous example, we now have $\xi(t) \approx (0.85)(0.2) \approx 0.017$, which provides a more reasonable quantification of the instantaneous synchronization considering the whole network.

D. Spectral Characterization

Given a time series or signal $s(t)$, it is often quite difficult to identify its periodical components. By reinforcing the intrinsic periodicities along the signal, its *autocorrelation* allows a more effective means for inferring its constituent oscillations. In this work we resource to the *power spectrum* $P(f)$ of the signal $s(t)$, which corresponds to the squared magnitude of the Fourier transform of the autocorrelation of $s(t)$ [46]. More specifically, given the signal $s(t)$, its Fourier transform is defined as

$$S(f) = \int_{t=-\infty}^{\infty} s(t) \exp(-i2\pi ft) dt$$

The autocorrelation of $s(t)$ is

$$a(\tau) = \int_{t=-\infty}^{\infty} s(t) s(\tau - t) dt$$

Therefore, the Fourier transform of the autocorrelation function is immediately given by the correlation theorem as

$$A(f) = S(f) S(f)^*$$

where ' $S(f)^*$ ' is the conjugate of S . The *magnitude of the spectrum* of $s(t)$ is

$$|A(f)| = \sqrt{S(f) S(f)^*}$$

The *power spectrum* of $s(t)$ is defined as being equal to the squared magnitude of the spectrum of $s(t)$, i.e.

$$P(f) = S(f) S(f)^*$$

The power spectrum allows the identification of auto-correlations (especially oscillations) of the original signal. More specifically, presence of peaks at specific frequencies f in the power spectrum indicate the presence of respective oscillations with frequency f in the original signal $s(t)$. All power spectra in this work are estimated by using the Fast Fourier Transform (FFT).

E. Multivariate Statistical Methods

The spikes produced along time for each neuron in the complex neuronal networks can be understood as *patterns*, which can be compared and classified by using multivariate statistics [46, 47, 48] and/or pattern recognition methods [46, 48]. In the present work, we apply the Principal Component Analysis (PCA) methodology [35, 46] in order to decorrelate the spike patterns [49] and to obtain more significant clusters in respective projections of the original patterns.

Given a set of M spike patterns along H time steps, a total of H measurements corresponding to the presence of a spike at each time can be obtained. Let us define the matrix U so that each of its rows corresponds to a train of spikes, so that U has dimension $M \times H$. Let $\vec{\mu}$ be the $1 \times H$ vector containing the average number of spikes at each time step $h = 1, 2, \dots, H$. Now, define the new matrix F as

$$F = U - \text{ones}(M, 1)\vec{\mu}$$

where $\text{ones}(M, 1)$ is a $M \times 1$ vector of ones. The *covariance matrix*, taking into account all pairwise covariances, is immediately given as

$$C = \frac{1}{M-1} FF^T$$

Observe that C is symmetric. Let λ_i be the eigenvalues of C sorted in descending order, with respective eigenvectors \vec{v}_i . The Karhunen-Loève transform of the original measurements is the stochastic linear transformation implemented by the matrix G given as follows

$$G = \begin{bmatrix} \leftarrow & \vec{v}_1 & \rightarrow \\ \leftarrow & \vec{v}_2 & \rightarrow \\ \dots & \dots & \dots \\ \leftarrow & \vec{v}_m & \rightarrow \end{bmatrix} \quad (4)$$

The PCA method involves transforming the original measurements as $V = GU^T$ with $m \ll H$, as allowed by the high redundancy normally found along and between signals. It can be shown that the resulting new measurements V , which correspond to linear combinations of the original measurements, are completely decorrelated by the PCA methodology, therefore maximizing the variation of the data along the first new variables.

III. MODELING AND SIMULATION

In this work, we focus attention on the two following specific features: (i) integrate-and-fire dynamics at each node; and (ii) conservation of incoming activation. Figure 1 shows the basic node adopted henceforth, which corresponds to a simple integrate-and-fire neuron. Each such node i includes $n(i)$ inputs and $m(i)$ outputs. The input activity is integrated until its value reaches the threshold $T(i)$ (hard limit non-linearity is adopted in this work), in which case the neuron fires.

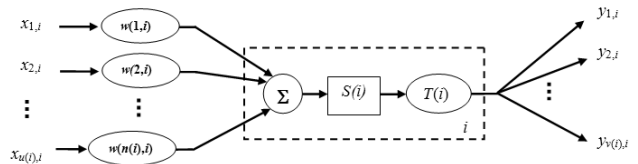


FIG. 1: The integrate-and-fire type of neuron adopted in this work.

The integrator and non-linear stages are henceforth understood to constitute the *soma* (or body) of the neuron. The above type of neuron can be immediately modified in order to allow the conservation of the total activation which has already entered the system (the system may involve sources of activation). First, once the neuron fires, all its stored activation is liberated through the outgoing edge (i.e. axons). Observe that the total liberated activation will be necessarily equal to the threshold $T(i)$, and that the activation will be divided amongst the outgoing edges, so that each receive a fraction of activation equal to $y_{i,j} = 1/k_{out}(i)$ (so, $k_{out}(i) = m(i)$). Second, the total activation received by the neuron is stored internally until the neuron fires. After each spike and transfer of the currently stored activation, the state of the neuron is cleared. These two simple modifications allow the activation which has already entered the system to be completely conserved along time. It should be observed that the division of activation amongst the outgoing connections is not biologically reasonable because the action potential in neurons involves signal reinforcement (the axon is active) and is known to produce spikes with similar intensities in most synapses. However, a biologically realistic network can be easily set up in order to reproduce the conservative dynamics by making the synapses at which the axons $y_{i,j}$ terminate to have weights $1/k_{out}(i)$.

In the case of the equilibrium analyses, the activation inside each memory $S(i)$ is limited to $L(i)$ at all times. This implies that the portion of the activation received by a node which exceeds $L(i)$ is discarded, therefore undermining the conservation of the activation received from the source node after the neurons start firing.

The complex neuronal networks considered in this article consist of a representative sample of each of the ER, BA, WS, GG, PN and PA models. The dynamics is implemented by considering each of the nodes in these networks to be a conservative integrate-and-fire neuron as discussed above. All neurons are assumed to have the same threshold $T = 1$. The activation of the network is implemented by assigning a source to a specified node, which therefore acts as a source of constant activation with intensity 1. As time passes, such an activation is distributed to the other nodes in the networks. The total of activated neurons at any time t is $N_a(t)$. In order to ensure activation conservation, the weight of each connection from node i to node j is defined as $w(j, i) = 1/k_{out}(i)$. For the sake of simplicity, each of the undirected edges yielded by the 6 considered network models are dissociated into one dendrite and one axon, so that the out-degree becomes identical to the in-degree. Less-symmetric configurations can be considered futrely. The *C. elegans* network is kept directed in our simulations.

The dynamics of such complex neuronal networks has been investigated with respect to: (a) the evolution of the activity of all nodes along time, represented in diagrams which are henceforth referred to as *activograms*; (b) the distribution of activated and non-activated nodes along time; (c) the distribution of the spikes produced by all neurons along time (*spikegram*); and (d) the evolution of the normalized instantaneous synchronization along time. The maximum NIS values obtained while considering the source at every node, as well as the time at which such values occur, are also considered in this work.

IV. TRANSIENT SYNCHRONIZATION: RESULTS AND DISCUSSION

Simulations on the theoretical models were performed considering $n = 100$ and $\langle k \rangle = 6$. The largest connected component in the neuronal network of *C. elegans* contained 239 neurons. For both the theoretical and real-world networks, each of the nodes was considered as a source of activation with intensity 1.

Figures 2 to 7 show the patterns of activation of all neurons for each time $t = 1, 2, \dots, 100$ obtained for each of the 6 networks by having the source of activation placed at node 50 (with a few exceptions, similar patterns were identified for the source at other nodes). More specifically, each of these figures show the activogram, i.e. the activation at each neuron along time (a), the active (white) and non-activate (black) neurons along time; and (c) the spikes produced by each neuron along time. The activations, instead of the normalized probabilities of activation, are shown in the activograms in all figures for the sake of better visualization.

A series of interesting results and interpretations can be identified from these figures. As expected, all acti-

vations tended to spread progressively from the source node 50 as time passes, with the rate of spikes increasing steadily with time. However, quite distinct patterns of activation have been observed for each of the considered networks. In the case of ER (Fig. 2), for instance, a reasonably uniform distribution of activation along time was obtained, with most nodes engaging into activity for the first time at similar instants (after approximately 10 or 20 steps, see Figure 2(b)). As shown in Fig. 3, quite a different dynamics of activation has been obtained for the BA network. Because of the presence of hubs, several nodes are activated relatively soon (less than 10 steps), while some nodes are only recruited much later. In addition, the activity along time tends to concentrate in the hubs at the left-hand side of the image. It would be particularly interesting to verify whether the rate of individual activations follow a power law. Yet another pattern of activations has been obtained for the WS model (Fig. 4), which has been made clearer by the fact that the original neurons in the one-dimensional regular lattice used to derive this network had been sequentially numbered. Now, the activation proceeds gradually through the successive neighbors. Also, once activated, the neurons seem to engage in more regular patterns of spiking than those obtained for ER and BA. The onset of activation in the GG network is peculiar, especially regarding the fact that neurons tend to start activity at the most diverse times. This is explained by the fact that the GG is not small-world, implying the activation to progress along the adjacencies along the network. Therefore, neurons which are connected to the source through longer shortest paths will engage into activity later. The activation diagrams obtained for the PN and PA networks are remarkably similar, being characterized by relatively uniform times for activation onset. This result is particularly surprising because these two networks are know to have markedly distinct structures [37, 38].

The normalized entropies of activations for each time considering all neurons, with source of activity at neuron 50, are shown in Figure 8. With a few exceptions, similar patterns were obtained when the activation source was placed at other neurons. These curves tend to be similar, involving an initial stage with plateaux of relatively low entropy, followed by more gradual progression to higher entropy approaching the maximum limit of $\log(N) \approx 4.61$ in all cases. Such initial plateaux are mainly a consequence of the distribution of activities among the axons of the neurons more immediately connected to the source, especially in the cases where the node associated to the source, or its more immediate neighbors, had large out-degree (recall that this implies the activity to be distributed amongst the outgoing edges). Figure 9 shows the normalized instantaneous synchronizations (NIS) obtained along time considering all neurons, with source of activation at node 50. Interestingly, after exhibiting some plateaux of synchronization at the initial time steps, these curves tend to evolve to a peak of synchronization and then decrease to near zero

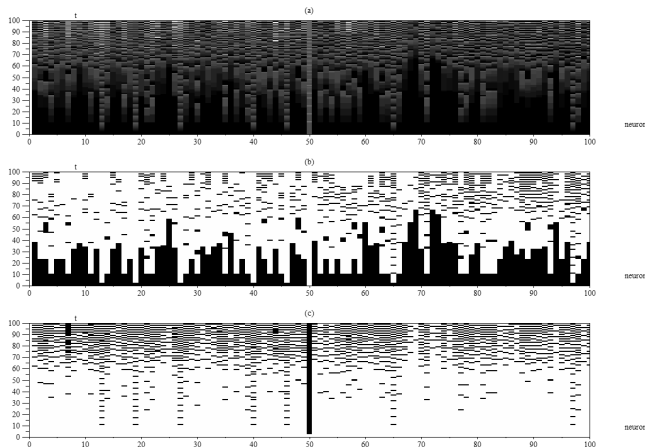


FIG. 2: Activation diagrams for ER network: (a) probability activation of each node along time (a); the active and non-activate neurons along time (b); and the spikes produced by each neuron along time (c). The source was placed at node 50.

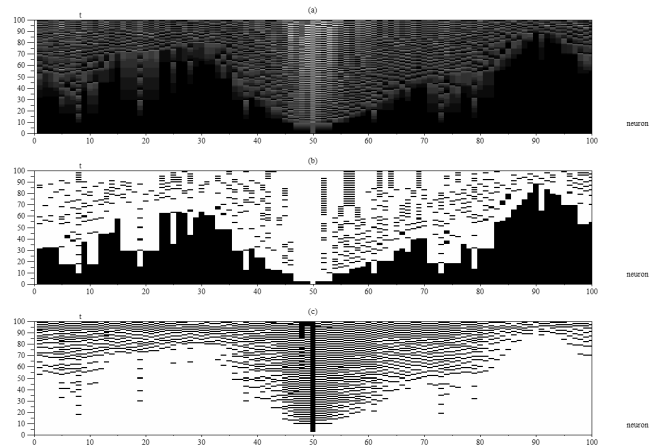


FIG. 4: Activation diagrams for WS network: (a) probability activation of each node along time (a); the active and non-activate neurons along time (b); and the spikes produced by each neuron along time (c). The source was placed at node 50.

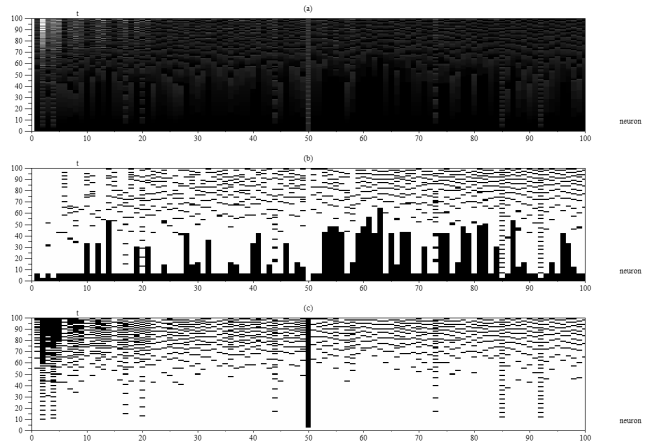


FIG. 3: Activation diagrams for BA network: (a) probability activation of each node along time (a); the active and non-activate neurons along time, shown in black (b); and the spikes produced by each neuron along time (c). The source was placed at node 50.

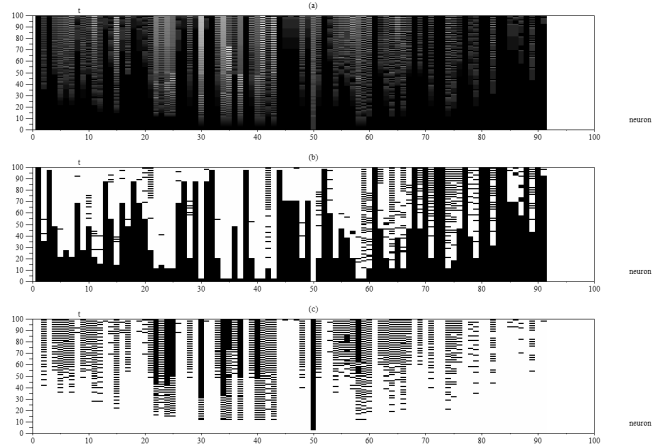


FIG. 5: Activation diagrams for GG network: (a) probability activation of each node along time (a); the active and non-activate neurons along time (b); and the spikes produced by each neuron along time (c). The source was placed at node 50.

activation (typically after 60 steps). Observe the higher values of NIS obtained for the BA network (Fig. 9b) and the more gradual decrease of NIS in the GG case (Fig. 9d).

A more complete picture of the instantaneous synchronization of the networks can be obtained by inspecting Figure 10, where the x -axes correspond to the maximum NIS obtained along all times, all nodes, and by considering the source in any node; while the y -axes show the time w at which the maximum NIS was obtained.

Remarkably, each of the networks led to relatively homogeneous maximum synchronization and time at which it occurred, defining reasonably dense clusters of points in these scatterplots. The times w at which the maximum synchronizations were observed are similar in all cases, except the GG network, and tend to be comprised within the interval from 1 to 30 steps. In the case of the GG, these times extend to 100 steps, reflecting the fact that the GG structure does not present the small-world. The highest synchronizations were observed for the BA,

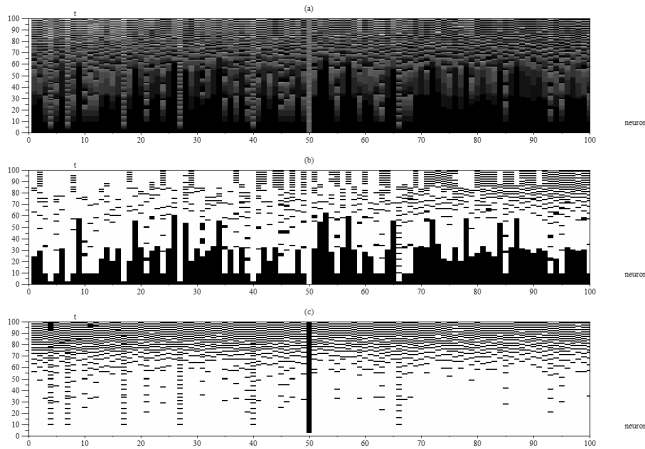


FIG. 6: Activation diagrams for PN network: (a) probability activation of each node along time (a); the active and non-active neurons along time (b); and the spikes produced by each neuron along time (c). The source was placed at node 50.

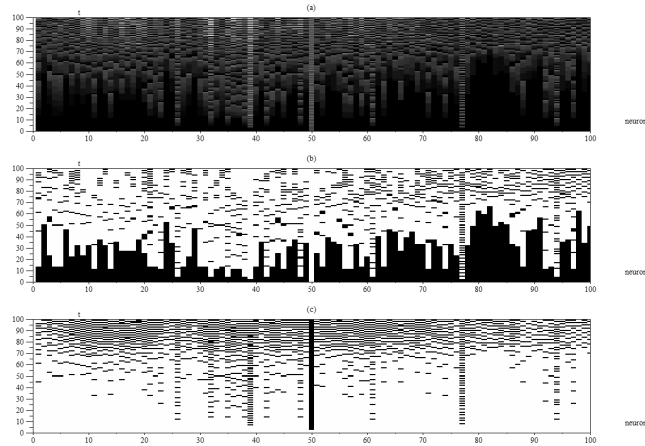


FIG. 7: Activation diagrams for PA network: (a) probability activation of each node along time (a); the active and non-active neurons along time (b); and the spikes produced by each neuron along time (c). The source was placed at node 50.

and the lowest for the WS and GG cases. The curves obtained for the PN and PA cases are similar one another and resemble the ER counterpart.

Figure 11 shows the normalized activations $a(i, t)$ at each of the nodes i of the considered GG network at time 100 (A) and 1000 (b), with the source of activation placed at node 50. Observe that the pattern of activation around the source tended to be similar in these two cases, suggesting that the activation tends to a steady-state which unfolds more strongly around the source. However, most

of the other activations changed almost completely along the time period between 100 and 1000 steps.

Figure 12 shows the activation diagrams (a), activated nodes (b) and spikes (c) obtained for all the 239 neurons of the *C. elegans* network along the 100 initial time steps, with the activation source at node 50. As can be clearly observed from Figure 12, most of the nodes are engaged in activity after only about 20 time steps. This seems to be related to the relatively high average node out-degree (14.36) of this network. Interestingly, the activation of the neurons seem to undergo an abrupt increase after approximately 100 steps, with most neurons presenting similar frequencies of activation thereafter. In addition, several neurons tended to exhibit similar frequency of spikes after such a transition. The peak of activation at the latest stages occurs at the maximum hub of this network (out-degree 73).

The evolutions of entropy and NIS along time with activations placed at nodes 1 to 50, shown in Figure 13, are particularly diversified, with initial plateaux presenting quite different lengths and heights. Interestingly, the lengthier plateaux also tended to yield the highest normalized instantaneous synchronization. Also noticeable are the shorter and lower plateaux which appear from time steps 1 to 20. However, after nearly 60 steps the synchronizations collapse.

The maximum NISs and respective times at which they occurred for the activation placed at each of the nodes in the *C. elegans* network are shown in Figure 14. It can be inferred from this figure that the *C. elegans* presents moderate values of maximum normalized instantaneous synchronizations, which occurs at an intensity comparable to that obtained for the ER, PN and PA networks. Interestingly, in some cases the maximum synchronization took place as late as at the 67th and 73th steps.

V. OSCILLATIONS IN UNIFORMLY-RANDOM NETWORKS

In this section we consider a series of complementary approaches in order to characterize the transient and equilibrium dynamics in two types of integrate-and-fire complex neuronal networks — namely ER and WS structure. Representative samples of each of these types of networks have been selected with sizes $N = 25, 50$ and 100 and average degrees $\langle k \rangle = 10, 20, 30, 40$ and 50.

Figure 15 shows the spikegrams obtained for the several configurations of ER networks. Observe the self-defined avalanche transitions at the beginning of the spikes obtained for all network configurations. In agreement with previous results [50], the avalanches initiation times were found to be quite similar for all network sizes, irrespectively of the average degree. The early spikes obtained for $N = 50$ and $\langle k \rangle = 10$; $N = 100$ and $\langle k \rangle = 10$; $N = 100$ and $\langle k \rangle = 20$ and $N = 100$; $\langle k \rangle = 30$ and $\langle k \rangle = 50$ were a consequence of the existence of communities which arise in the ER networks arising from ran-

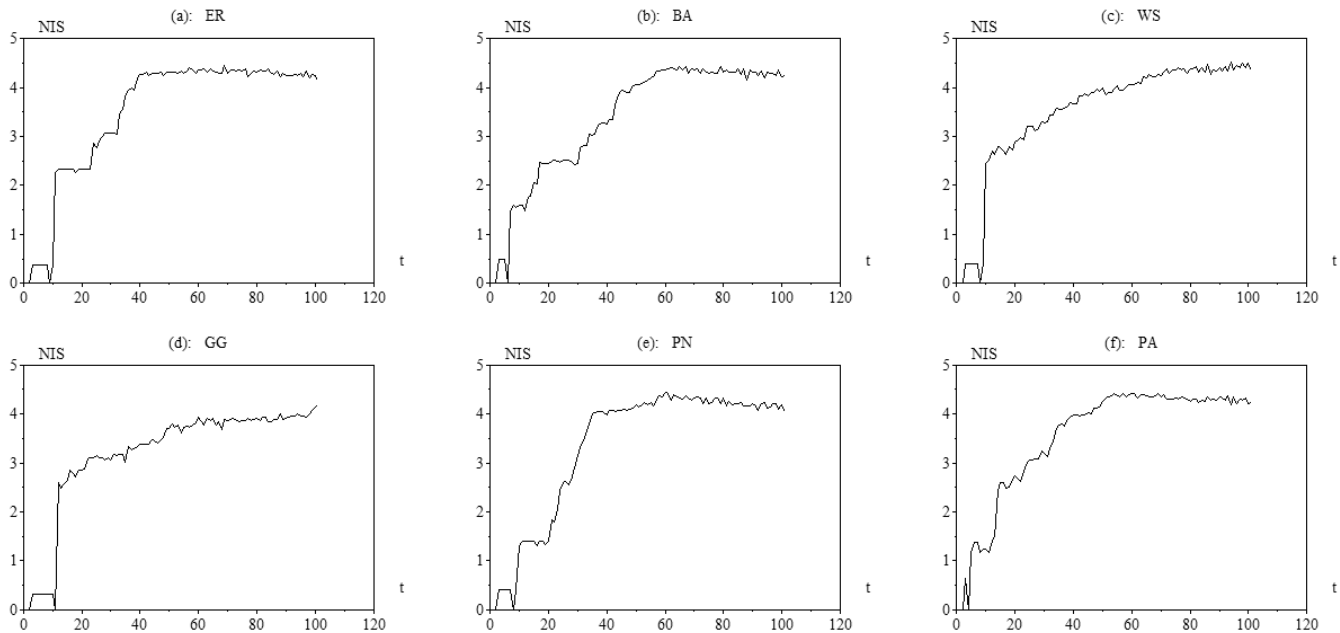


FIG. 8: The normalized entropy of the activations along time for each of the considered networks. The source was placed at node 50.

dom fluctuations. Interestingly, the oscillations tended to become more regular (more similar frequencies) and synchronized with the increase of the average degree. The routes to regularity and synchronization this parameter is increased exhibited groups of neurons producing similar spiking patterns.

The total number of spikes, shown in Figure 16 reflects the ensemble behavior of the respective complex neuronal networks, arising as a consequence of the linear superposition of the spikes being produced by each neuron (analogous to EEG potentials). The avalanche transitions can be clearly identified, taking place after nearly 40 steps for $N = 25$, 40 steps for $N = 50$ and 80 steps for $N = 100$, which confirms the previous study reported in [50]. In several cases, a clear intense peak is observed at the avalanche time, which is followed by oscillations whose regularity tend to increase with the average degree.

In addition to the total number of spikes, it is also important to take into account the respective power spectra, which are shown in Figure 17. Only the second half of each signal (number os spikes) has been considered for the calculation of the power spectra in order to represent the equilibrium regime. So, a total $H = 500$ time steps have been considered for the estimation of each spectrum.

Relatively rich spectral composition can be observed for most cases, suggesting particularly complex behavior of the oscillatory components. The progressive elimination of frequencies with the increase of the average degree is evident from Figure 17, especially for $N = 50$

and $N = 100$. In addition, the peaks of the spectra for $N = 50$ and $N = 100$ tend to appear near 20 and 10 frequency units, respectively. At the same time, it should be observed that the peaks of the spectra in Figure 17 tend to shift to the right-hand side for larger values of the average degree, signaling the increase of the main frequencies. The more regular oscillations obtained for larger average degrees are related to the fact that the higher this parameter, the more regular the degrees of the networks become. At the limit, for very large average degree, all nodes become connected, implying a highly regular structure as far as all possible topological features are concerned.

Unlike in the previous works [45, 50, 51, 52, 53], the activation inside each neuron is limited to the respective maximum value $L(i)$. In addition to being more biologically-realistic, such a choice also allowed particularly interesting oscillatory dynamics. At the same time, the limitation of the internal activation implies that the overall activation, constantly received from the source node, is no longer guaranteed to be conserved. It is therefore interesting to consider the total activation inside the whole complex neuronal networks along time. Such a measurement is depicted in Figure 18. Interestingly, two clearly distinct regimes are immediately identified: one transient period in which the internal activation increases linearly, followed by the steady-state regime characterized by nearly constant activation (even though activation is continuously pumped into the system through the source node). The transition between these two regimes

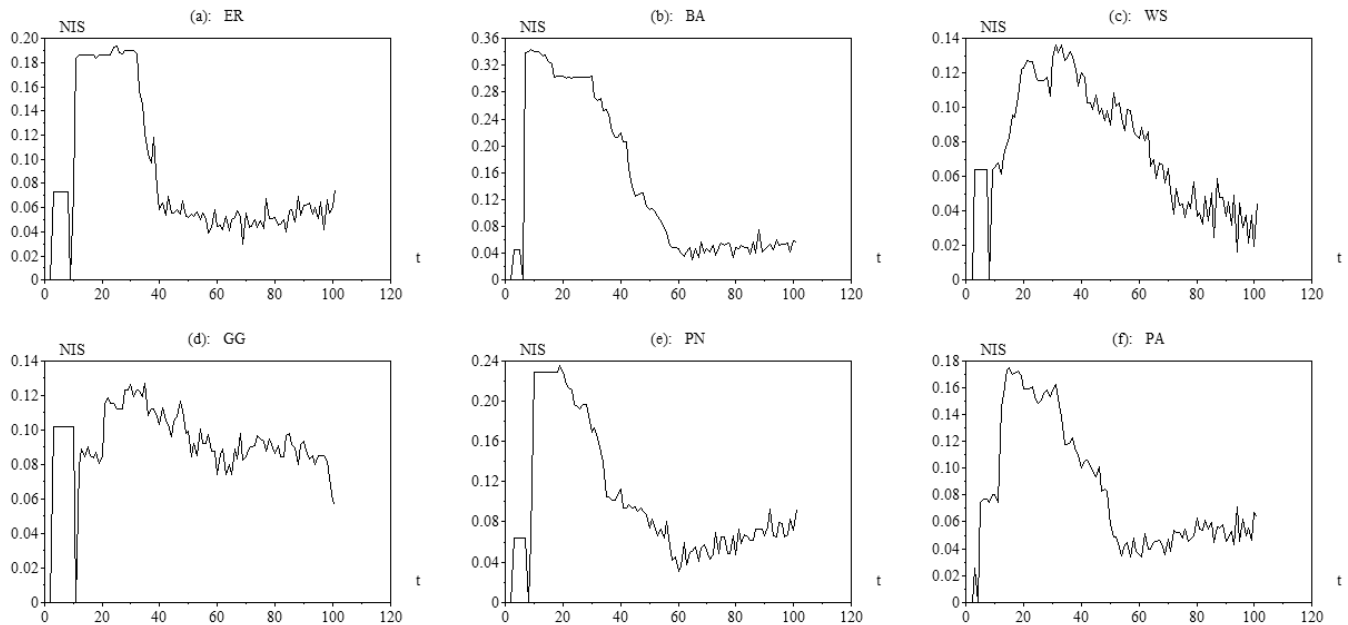


FIG. 9: The normalized instantaneous synchronization (NIS) along time for each of the considered networks. The source was placed at node 50.

is in most cases characterized by one abrupt surge of activation, related to the main avalanche. Such a result suggests that the main avalanche represents watershed *signaling the transition of the dynamics in the system from conservative to dissipative*.

Because the train of spikes produced by each individual neuron, shown in Figure 15, seems to be organized in clusters during the route towards more regular and synchronous firing (i.e. similar trains of spikes are obtained for groups of neurons), it is interesting to investigate such a possibility further. We do this with the help of the PCA method, which produced the results shown in Figure 19.

It is clear from this figure that the increase of the average node degree tends to produce denser groups of spiking patterns. At the same time, interesting clustering structures are obtained for small average node degrees, incorporating a dense central cluster (e.g. the PCA scatterplots for $N = 25$ and $\langle k \rangle = 10$, $N = 50$ and $\langle k \rangle = 10$, and $N = 100$ and $\langle k \rangle = 10$) surrounded by outliers. The dense cluster of spiking patterns tend to survive even for relatively large average degrees in the case of $N = 100$.

The correlations between the total number of spikes produced by each neuron during the simulations and the respective degrees have also been considered, yielding some of the most interesting results reported in the present work. These scatterplots are shown in Figure 20. Striking twin-linear correlation patterns have been obtained throughout. Such scatterplots indicate that a node with a given degree can spike at two distinct frequencies of spikes, with the number of spikes being lin-

early related to the node degrees. At the same time, given one of such rules, the number of spikes (i.e frequency) tends to be correlated with the degree of the original nodes. Such twin correlations are likely to be related to clusters of original nodes appearing at different concentric hierarchical levels, as discussed further in Section IX.

VI. OSCILLATIONS IN SMALL-WORLD NETWORKS

Having obtained a comprehensive characterization of the oscillations induced along the equilibrium regime in ER networks, it is interesting to shift our attention to the steady-state dynamics of WS integrate-and-fire activations. Figure 21 shows the spikegrams obtained for the several parametric configurations of the WS models.

Several interesting features are evident from the results shown in Figure 21. Foremost are the more gradual avalanches, which tend to be centralized around the source node (node 1) [55]. Longer avalanche initiation times are implied by larger network sizes N . Because the increase of the average degree implies more degree-regular networks, the gradual activation of the neurons observed for relatively smaller average node degrees became sharper for larger average node degrees. As with the ER cases, the spiking patterns also tended to become more regular and synchronized for larger values of average degree.

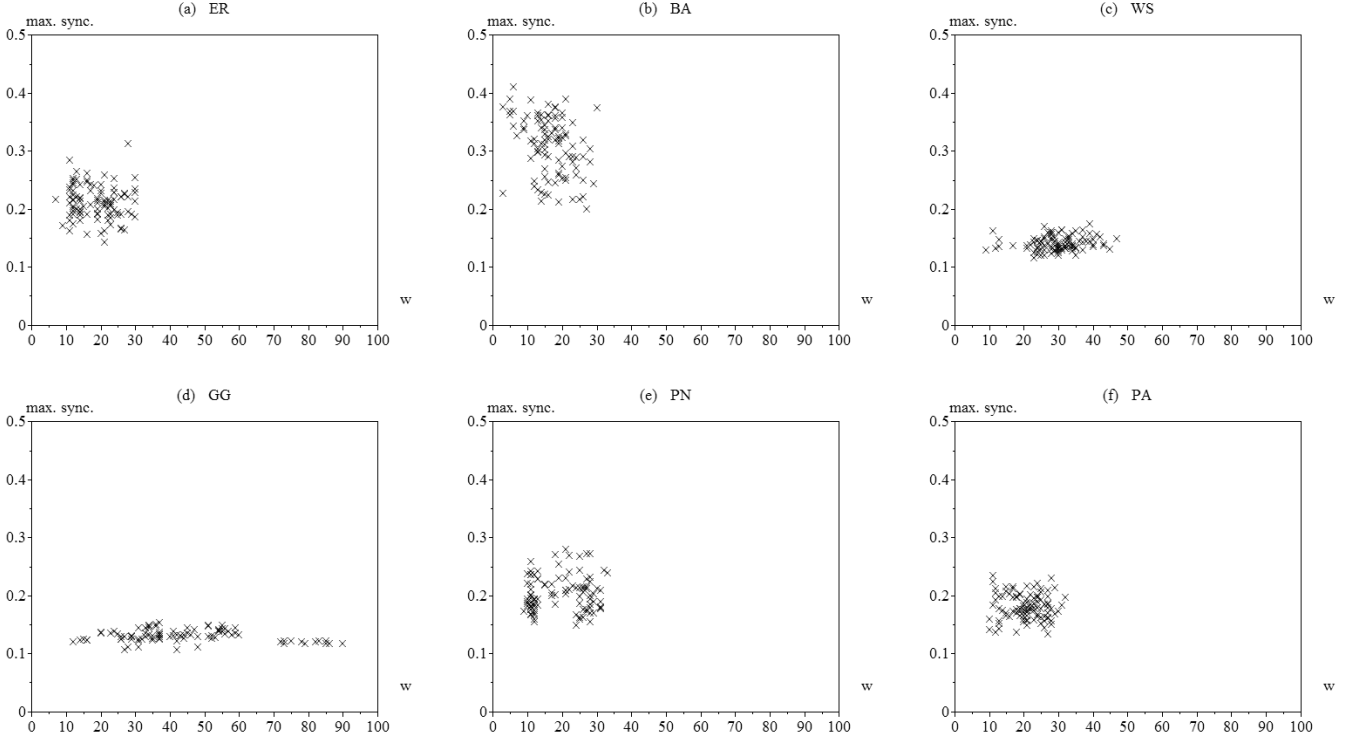


FIG. 10: Scatterplots of the maximum NIS (y -axes) and time at which it manifested itself (x -axes) obtained for each networks by considering activations at each possible node.

Figure 22 depicts the power spectra obtained for each of the considered WS configurations. Such spectra, which were obtained by considering the equilibrium regime of the spikings (i.e. the time steps from 500 to 1000) are remarkably similar to those obtained by the ER structures (Fig. 17, suggesting some possible universality between different complex networks types).

Regarding the total activation inside the system, the revealed results (not shown in this work) also included the two regimes as in the ER case, but with sublinear increase during the transient regime, which was also duly followed by the dissipative plateau of overall activation.

Figure 20 shows the scatterplots of the original node degrees and total number of spikes induced by each individual neuronal cell. Though these two features also tended to be organized in terms of parallel straight groups for small values of average degree, the correlations are now substantially less definite.

VII. THE EQUIVALENT MODEL FOR NON-UNIFORM DEGREES

Figure 24 illustrates the procedure which had to be adopted in order to obtain the a more effective version of the equivalent model of complex networks, by taking into

account non-uniformities of degrees amongst the original nodes. First, the hierarchical organization of the original network with reference to a given node i is obtained (Fig 24). In this specific case we have 5 concentric levels ($h = 0, 1, \dots, H = 4$), each containing 1, 3, 6, 2 and 1 nodes (i.e. $n_0(i) = 1$; $n_1(3) = 1$; $n_2(i) = 6$; $n_3(i) = 2$; $n_4(i) = 1$). The nodes within each concentric level which have identical degrees are then subsumed into equivalent nodes. Thus, nodes 3 and 4 at level $h = 1$ — all with degree equal to 5 — become associated to the equivalent node **B**. Nodes 5, 6 and 7, which have degree 4, are subsumed by node **F**. The topology of the resulting equivalent model is illustrated in Figure reffig:equiv.

Now, the weights associated to the edges in the equivalent structure in Figure 24 are determined, similarly as done in [45], by means of the following equation, applied to each pair of equivalent nodes v and p

$$W(v, p) = k(v, p)/d$$

where $k(v, p)$ is the number of original edges going from the nodes associated to the equivalent node p to the nodes associated to the equivalent node v , $d = \sum_{g \in \Omega(p)} k(g, p)$ and $\Omega(p)$ is the set of equivalent nodes that receive a directed edge from p . Observe that $W(b, a)$ expresses the weight of the connection from a to b . The weights there-

fore obtained for the graph in Figure 24 are given as follows

$$W = \begin{bmatrix} 0 & 1/5 & 1/3 & 0 & 0 & 0 & 0 \\ 2/3 & 1/5 & 0 & 1/2 & 1/4 & 0 & 0 \\ 1/3 & 0 & 0 & 0 & 1/8 & 0 & 0 \\ 0 & 1/5 & 0 & 0 & 0 & 0 & 0 \\ 0 & 2/5 & 0 & 0 & 1/4 & 4/6 & 0 \\ 0 & 0 & 2/3 & 0 & 3/8 & 1/6 & 1 \\ 0 & 0 & 0 & 1/2 & 0 & 1/6 & 0 \end{bmatrix}$$

For instance, as the two original nodes associated to the equivalent node **B**, both of which with degree 5, send two edges to the equivalent node **A**, two edges to **D**, four edges to **E**, while two edges remain inside **B**, we have $W(A, B) = 1/5$; $W(D, B) = 1/5$; $W(E, B) = 2/5$; $W(B, B) = 1/5$.

The thresholds associated to neuron corresponding to each equivalent node are immediately given as the number of original nodes associated to that equivalent node. Therefore, we have that $T(A) = 1$; $T(B) = 2$; $T(C) = 1$; $T(D) = 2$; $T(E) = 1$; $T(F) = 3$; $T(G) = 2$; and $T(H) = 1$. The limitations to the activations stored into each memory are also set as being equal to the respective number of nodes within each equivalent node, i.e. $T(i) = L(i)$. Observe that the so-obtained equivalent network itself correspond to an integrate-and-fire complex neuronal networks with varying thresholds.

VIII. EQUIVALENT MODEL PREDICTIONS

Having characterized the oscillatory integrate-and-fire dynamics along the transient and equilibrium regimes in terms of several measurements, it is time to consider the respective equivalent models. The importance of such an approach lies in the fact that these structures involve a fraction of the original number of nodes, therefore allowing the identification and theoretical modeling of more definite relationships between structure and dynamics. We start by considering the distribution of the equivalent nodes and weights, as well as by comparing the predicted and real number of spikes and spectra for ER.

Tables I and II give several features of the topological structure of the equivalent models obtained for each of the ER and WS configurations, respectively. These features include the total number of original nodes in each concentric level (upper line), the hierarchical degrees (second line), the total number of equivalent nodes (in bold, third line), and the number of equivalent nodes per concentric level (within brackets, third line). It is clear from such measurements that the WS structure implied a larger number of concentric levels in all cases. On the other hand, most of the ER structures implied two or three levels (the first of each level corresponding to the source node), except for the network with $N = 100$ and $\langle k \rangle = 10$, which implied 4 concentric levels. Also, because

of its greater degree uniformity, the WS model yielded substantially fewer equivalent nodes than the ER structures. The relatively large number of equivalent nodes obtained for each concentric level confirms the fact that these two types of supposedly regular networks do actually a wide dispersion of node degrees, especially in the case of the ER configurations. That is the reason why equivalent models which do not take into account such a heterogeneity cannot yield accurate predictions.

Though the partitioning of the concentric levels in terms of groups of nodes with identical degrees was critical for proper modeling of the oscillatory dynamics, it supplied as byproduct a new hierarchical measurement corresponding to the number of nodes with specific degrees at each concentric level. Because such features have been presently found to be essential for the integrate-and-fire dynamics, it is likely that they will also provide valuable resources for the characterization of the topology of the networks.

The weights of the equivalent models obtained for each of the ER configurations are shown in Figure 25. The equivalent nodes are organized bottom-upwards along the columns and rows according to increasing degrees of the respectively subsumed original nodes. It is clear from these matrices that there are some equivalent nodes which receive converging intense weights (the clearer rows in the matrices — recall that we adopt the convention that the edges extend from the columns towards the rows). Such nodes are particularly important for the non-linear dynamics because of their greater tendency to spike, defining the main avalanches.

We now present some predictions of the dynamical features as obtained by using the respective equivalent models. Figure 26 shows the number of spikes predicted by the equivalent model for all the considered ER configurations. By comparing with the respective real number of spikes shown in Figure 16, it becomes clear that the equivalent model allowed an impressive estimation of both the transient and steady-state dynamics in every case.

Similarly impressive predictions of several aspects of the dynamics, including spectra, were also obtained for the WS configurations but are not shown here.

IX. EQUILIBRIUM CONFIGURATIONS: OVERALL DISCUSSION

At this point, after having characterized several aspects of the integrate-and-fire dynamics obtained for the original networks, as well as the features of the respective equivalent models and predictions, it is time to integrate all such information in order to obtain a more comprehensive explanation of the origin and properties of the oscillations observed for the integrate-and-fire complex neuronal networks.

The two clusters of correlations observed for the ER model (Fig. 20) are particularly relevant, suggesting that

	$\langle k \rangle = 10$	$\langle k \rangle = 20$	$\langle k \rangle = 30$	$\langle k \rangle = 40$	$\langle k \rangle = 50$
$N = 25$	1, 17, 7 17, 72, 0 16: (1) (10) (5)	1, 23, 1 23, 23, 0 5: (1) (3) (1)	1, 24 24, 0 2: (1) (1)	1, 24 24, 0 2: (1) (1)	1, 24 24, 0 2: (1) (1)
$N = 50$	1, 14, 35 14, 168, 0 23: (1) (10) (12)	1, 35, 14 35, 310, 0 22: (1) (13) (8)	1, 42, 7 42, 246, 0 17: (1) (12) (4)	1, 45, 4 45, 176, 0 9: (1) (6) (2)	1, 49 49, 0 2: (1) (1)
$N = 100$	1, 12, 83, 4 12, 189, 80, 0 31: (1) (9) (17) (4)	1, 36, 63 36, 859, 0 34: (1) (15) (18)	1, 67, 32 67, 1117, 0 33: (1) (19) (13)	1, 68, 31 68, 1333, 0 36: (1) (20) (15)	1, 75, 24 75, 1358, 0 34: (1) (20) (13)

TABLE I: Features of the equivalent models obtained for the ER configurations: number of nodes per level (first line); hierarchical degrees of each level (second line); and total number of equivalent nodes (bold, third line) and the number of equivalent per concentric level (within brackets).

	$\langle k \rangle = 10$	$\langle k \rangle = 20$	$\langle k \rangle = 30$	$\langle k \rangle = 40$	$\langle k \rangle = 50$
$N = 25$	1, 10, 12, 2 10, 32, 15, 0 9: (1) (2) (4) (2)	1, 18, 6 18, 84, 0 10: (1) (6) (3)	1, 21, 3 21, 54, 0 9: (1) (5) (3)	1, 23, 1 23, 21, 0 8: (1) (6) (1)	1, 21, 3 21, 57, 0 10: (1) (6) (3)
$N = 50$	1, 9, 14, 24, 2 9, 36, 54, 17, 0 15: (1) (4) (4) (4) (2)	1, 19, 26, 4 19, 131, 62, 0 17: (1) (6) (8) (2)	1, 28, 21 28, 271, 0 16: (1) (8) (7)	1, 38, 11 38, 309, 0 16: (1) (9) (6)	1, 46, 3 46, 114, 0 12: (1) (8) (3)
$N = 100$	1, 11, 34, 38, 16 11, 57, 118, 91, 0 18: (1) (3) (4) (6) (4)	1, 21, 57, 21 21, 179, 260, 0 21: (1) (7) (9) (4)	1, 27, 55, 1 27, 312, 338, 0 23: (1) (8) (9) (5)	1, 42, 57 42, 577, 0 22: (1) (11) (10)	1, 50, 49 50, 843, 0 19: (1) (9) (9)

TABLE II: Features of the equivalent models obtained for the WS configurations: number of nodes per level (first line); hierarchical degrees of each level (second line); and total number of equivalent nodes (bold, third line) and the number of equivalent per concentric level (within brackets).

the spiking frequency tends to increase linearly with the indegree of the neurons. Indeed, the higher the indegree, the more activation a neuron will receive along time, enhancing its chance of firing. Interestingly, the nodes belonging to each of the two groups straight correlations in (Fig. 20) have been found to belong to distinct respective hierarchical levels. As the neurons at different concentric levels tend to fire with different frequencies, depending on their respective number of nodes and connections, the two groups of correlations are obtained, with the intra-group straight dispersions being accounted by the above observed tendency of the spiking frequency to increase linearly with the indegrees.

Despite the clear separation of the hierarchical levels provided by the correlation diagrams in Figure 20, it is remarkable that the spiking patterns in Figure 19 failed completely to clusterize with respect to the hierarchies. This interesting fact can be taken as an indication that though the nodes belonging to different hierarchical levels do present a well-defined *mean frequency*, they are highly irregular as far as the interspike times are concerned. This can indeed be corroborated by the visual analysis of the spikegrams in Figure 15 as well as from the rich spectra (in the sense of exhibiting many frequencies) shown in Figure 17. With this respect, it would be

interesting to consider PCA projections taking into account smoothed versions of the spiking patterns, which would enhance the correlations between those patterns and perhaps make more evident the hierarchical clusters.

Because the considered WS structures implied larger number of hierarchical levels (see Tab. II), with respective neurons firing at distinct group frequencies, the linear relationship between the spiking frequency and the indegree became blurred in the respective scatterplots in Figure 23.

X. CONCLUDING REMARKS

A. Transient Synchronization

The subjects of complex networks, neuronal networks and synchronization have special importance in the investigation of complex systems and natural phenomena. The current work has brought these three issues together with respect to transient non-linear dynamics unfolding in complex networks with different structures and conservation of activation. More specifically, the normalized instantaneous synchronization (NIS) has been proposed as a measurement of the instantaneous synchronization of

the dynamics among the nodes in the networks at each specific time. The activation of the networks was performed by placing a source of unitary activity at each specific node, and the respective dynamics observed and characterized in terms of the maximum NIS values, as well as the respective times when they occurred.

The obtained results indicate that the normalized instantaneous synchronization tends to increase along the initial steps and then collapse. Also, the intrinsic topological organization of each of the considered types of networks was verified to imply markedly diverse patterns of activation and maximum NIS. While relatively uniform patterns of activation spreading were observed for the ER model, groups of hubs tended to concentrate the activity in BA networks. Also, the onset of activation of nodes was verified to be more uniform for the ER case than for BA. The WS structure yielded a pattern of activation which tended to spread gradually amongst the neighbors of the source. Similar activation and synchronization were observed for the two knitted networks, namely PN and PA. This is particularly surprising because, though both these networks are defined in terms of paths, they have completely different degrees of regularity [37, 38]. The different networks also implied distinct maximum NISs, with the BA resulting more synchronized along the transient dynamics of activation. Quite diverse times of maximum activation were observed for the geographical network. Regarding the *C. elegans* network, it was found to exhibit diverse dynamics with respect to the position of the source. In addition, most nodes tended to start activity with remarkable uniformity during the initial 20 time steps. The overall activation in this network underwent an abrupt increase after nearly 100 time steps. At the longest term, the hubs tended to dominate the activation dynamics. It is interesting to observe that the approaches developed in this work are relevant not only for the synchronization studies, but also for the characterization of the activation in non-linear systems underlain by complex connectivity.

The perspectives for future investigations are varied. Among the possibilities, it would be interesting to consider other types of activations, e.g. involving sources at more than one node or periodic activation instead of the constant values used in this work. It would be particularly interesting to study the combined potential of specific sources for defining diverse dynamical features of the neuronal activity, especially regarding the facilitation of one source of activation by other sources. Another possibility is to consider the synchronizability of the rates of accesses to a specific node from activity originating at several nodes [20]. Such investigation, which is allowed by the conservation of activity [56], would involve the identification of the original source of activations, as well as its displacement along the networks, during the dissemination of the activation. Other interesting questions concern the instant frequency of spiking along time for each node, as well as the quantification of correlations and other types of relationships between the acti-

vations. Because the activation of most of the considered networks tends to undergo an abrupt dissemination after an initial transient period, it would be interesting to investigate for possible critical dynamics (e.g. phase transition). It would also be useful to characterize the steady state of activations. Although the concepts and methods reported in this article have been considered from the specific perspective of neuronal networks, they can be immediately extended to investigations of other situations such as those involving cortical and biological systems, particularly gene activation and protein synthesis.

B. Equilibrium Synchronization

Though relatively simple, the integrate-and-fire model yields rich dynamical features, including avalanches, activation confinement inside communities and oscillations. Having addressed and explained the first two phenomena by using equivalent models [45, 50], it is now interesting to consider the origins and properties of the oscillations observed at both transient and equilibrium regimes in integrate-and-fire complex neuronal networks. This constituted precisely the objective of the present work. Its main contributions are reviewed and discussed as follows.

Characterization of Several Aspects of the Oscillations: The oscillations in the integrate-and-fire complex neuronal networks were characterized in terms of several measurements and approaches, including the visualization of the spikegrams, the total number of spikes along time and respective power spectra, total activation along time, PCA decorrelation of the spiking patterns in order to seek for clusterized dynamics features, as well as correlations between the total number of spikes and degrees of each neuron. Each of these approaches allowed interesting complementary insights about the oscillatory behavior in uniformly-random (ER) and small-world (WS) configurations. Particularly revealing were the twin correlations observed for both models, which were found to correspond to different frequencies of oscillations taking place at different concentric levels of the networks. Such correlations also indicated that the mean spiking frequency is linearly related to the indegree of the respective neurons, which constitutes a particularly relevant property of the analyzed structures. Analogously to the investigation of linear diffusive dynamics reported in [54], this property links structure and oscillatory dynamics, implying that topological hubs will also become hubs of activity in the integrate-and-fire dynamics. The scatterplots obtained by the PCA projection of the individual spiking patterns yielded interesting structures which, however, were not in correspondence with the twin-correlation partitionings. The spectra, rich in frequencies, confirmed the complex structure of the spikings.

Identification of Two Clearly-Defined Regimes: The consideration of the total activation along time re-

vealed two distinct and well-defined regimes: a conservative transient period, followed by the dissipative steady-state regime. The critical point separating these two dynamics was found to correspond to the main avalanches. The transient evolution was found to be more gradual for the WS configurations, which could be indeed expected because of the less pronounced (if any) avalanches in this type of networks.

Equivalent Model for Non-Uniform Degrees:

Following the comprehensive characterization of the oscillatory properties of the integrate-and-fire dynamics in complex neuronal networks, an enhanced equivalent model was developed which takes into account the diversity of degrees within each concentric topological level. More specifically, the nodes with identical degrees at each of the levels are associated to respective equivalent nodes, allowing a more detailed model. Such a modification was found to be critical for paving the way to impressively accurate predictions of both the transient and steady-state features of the non-linear dynamics.

Limitation of the Stored Activation: Differently from the previous approaches reported in [45, 50, 51, 52, 53], the activation stored inside the state (memory) of each neuron was limited to be at most equal to the respective threshold. In addition to being more biologically-realistic in which concerns neuronal networks, this choice also allowed more interesting oscillatory dynamics.

Additional Hierarchical Measurements of Network Topology: In addition to paving the way for precise estimations of the dynamics, the enhanced equivalent model also yielded as a byproduct new hierarchical measurements corresponding to the number of nodes with specific degrees found at each of the respective concentric levels. Because such topological features proved to be fundamental for modeling the non-linear integrate-and-fire dynamics, it is expected that they can also provide valuable features for the characterization and classification of complex networks [35].

Identification of the Origin and Properties of Oscillations: As a consequence of the comprehensive characterization and modeling of the integrate-and-fire dynamics, a better understanding of the origins and properties of the spiking oscillations have been achieved. Of special importance are the positive correlations between the mean spiking frequency and the neuron indegrees and the fact that nodes at distinct concentric levels tend to fire with different ensemble frequencies. The combination of these two effects yielded the remarkable twin-correlation diagrams. In addition, it has been found that the oscillations tend to unfold after the main avalanches, i.e. along the steady-state of the dynamics, as revealed by the total activation in terms of time.

Several are the possibilities for further related investigations. In principle, most of the suggestions for future work identified in [45, 50, 51, 52, 53] can be immediately extended to the present work. More specific possibilities for further investigations are identified and briefly discussed in the following.

Further Simplifications by Considering Degree Intervals: It would be interesting to consider the subsuming of the nodes in each concentric level not strictly under the condition of identical degrees, but by having similar degrees (i.e. comprised within specific intervals). Such a modification would immediately contribute to a further reduction of the overall number of equivalent nodes, making the equivalent models more compact. It would be interesting to quantify the effect of such a simplification on the accuracy of the respective predictions of the dynamical features.

Modular Equivalent Model with Non-Uniform Degrees: Because of the finer level of representation allowed by the currently reported equivalent model, it would be potentially useful to extend the previous equivalent models used to explain and predict avalanches and activation confinement inside communities.

Oscillation Analysis with Action Potentials: While the current work, analogously to the previous works [45, 50, 51, 52, 53], considered the activation of each spike to be equally distributed amongst the outgoing edges (i.e. axons), it would be interesting to consider the more biologically-realistic hypothesis that the spikes have constant amplitude (action potential). Preliminary investigations have already indicated that avalanches, activation confinement and oscillations are all present in this type of non-linear dynamics. However, it would be interesting to perform more systematic related investigations.

Chaos and Chaos Control: The particularly complex spiking patterns obtained after the main avalanche suggest that the dynamics of the considered networks may be chaotic. It would be particularly promising to apply methods from dynamics systems, such as delay diagrams and fractal dimensions, in order to search for chaotic behavior in the integrate-and-fire complex neuronal networks. Another interesting perspective would be to apply concepts from chaos control in order to interfere with the several remarkable aspects of the investigated dynamics.

Distinct Weights: So far, we have been limited to integrate-and-fire complex neuronal networks containing identical weights. Indeed, the weights have only been used in order to obtain the respective equivalent models. In this case, the weights correspond to the proportions of the activations (edges) which are sent to each equivalent node. It would be interesting to consider complex neuronal networks incorporating weights, in order to investigate the effects of such distributions on the respective dynamics.

Investigation of Oscillations in Other Theoretical Complex Networks Models: Because of space restrictions, the oscillatory behavior of integrate-and-fire complex neuronal networks described in this work has been restricted to a uniformly-random and a small-world theoretical models of complex networks. It would be particularly promising to extend such an investigation to other important types of network topologies, especially

scale free and geographical. The consideration of the highly regular knitted structures [37] would also be interesting.

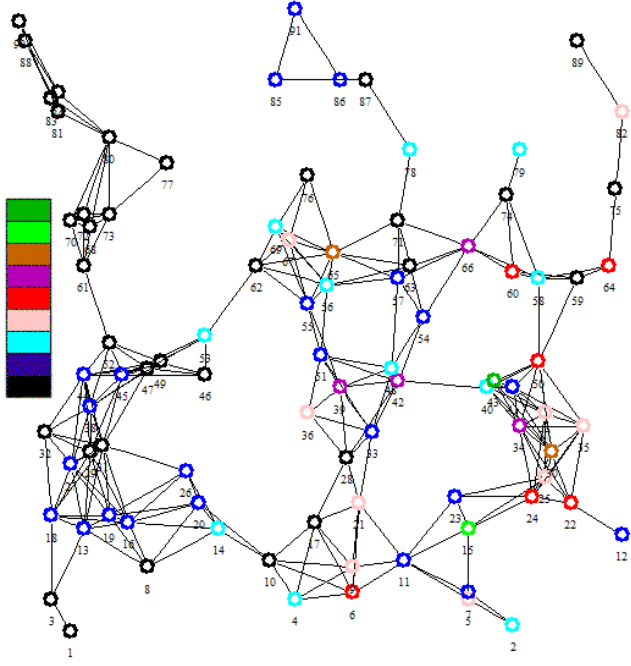
Applications to Real-World Problems: Though we have so far considered the oscillations in theoretical models of complex neuronal networks, the respective concepts and methods are immediately applicable to real-world networks. Of particular interest would be to characterize and model the neuronal network of *C. elegans*,

as well as cortical networks.

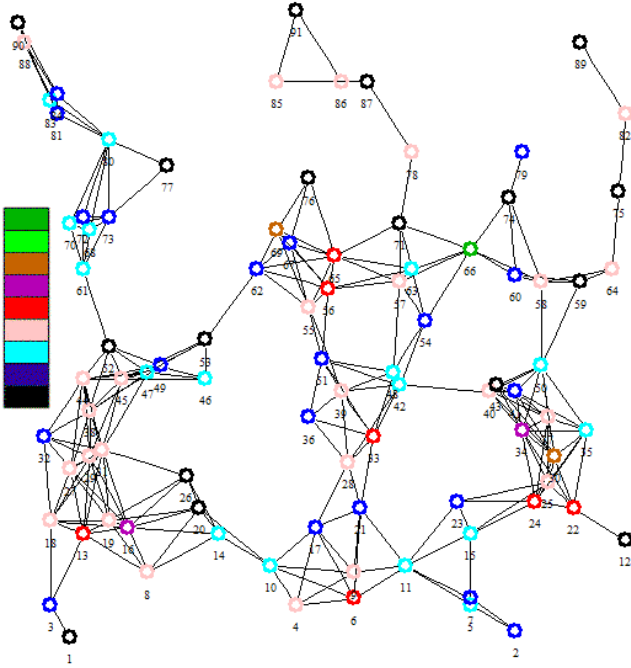
Acknowledgments

Luciano da F. Costa thanks CNPq (308231/03-1) and FAPESP (05/00587-5) for sponsorship.

-
- [1] D. Stauffer, L. Aharony, L. da F. Costa, and J. Adler, Eur. Phys. J. B **32**, 395 (2003).
- [2] L. da F. Costa and D. Stauffer, Physica A **330**, 37 (2003).
- [3] L. da F. Costa (2005), arXiv:q-bio/0503041.
- [4] B. J. Kim, Phys. Rev. E **69**, 045101 (2004).
- [5] R. M. Memmesheimer and M. Timme, Physica D **224**, 182 (2006).
- [6] D. J. Watts and S. H. Strogatz, Nature **393**, 409 (1998).
- [7] D. Watts, *Small Worlds: The Dynamics of Networks between Order and Randomness* (Princeton University Press, 2003).
- [8] D. Watts, *Six Degrees: The Science of a Connected Age* (W. W. Norton and Company, 2004).
- [9] S. Boccaletti, V. Latora, Y. Moreno, M. Chavez, and D. Hwang, Phys. Rep. **424**, 175 (2006).
- [10] H. Hong, B. J. Kim, M. Y. Choi, and H. Park, Phys. Rev. E **69**, 067105 (2004).
- [11] D. S. Lee, Phys. Rev. E **72**, 026208 (2005).
- [12] D. U. Hwang, M. Chavez, A. Amann, and S. Boccaletti, Phys. Rev. Letts. **94**, 138701 (2005).
- [13] C. Zhou, A. E. Motter, and J. Kurths, Phys. Rev. Letts. **96**, 034101 (2006).
- [14] S. Boccaletti, M. Ivachenko, V. Latora, A. Pluchino, and A. Rapisarda, Phys. Rev. E **75**, 045102 (2007).
- [15] I. Lodato, S. Boccaletti, and V. Latora, Phys. Rev. Letts **78**, 28001 (2007).
- [16] T. Nishiwaka and A. E. Motter, Phys. D **224**, 77 (2006).
- [17] F. Sorrentino, M. di Bernardo, F. Garofalo, and G. Chen, Phys. Rev. E **75**, 046103 (2007).
- [18] F. Sorrentino and E. Ott, Phys. Rev. E **76**, 056114 (2007).
- [19] J. A. Almendral and A. D. Guilerá (2007), arXiv:0705.3216.
- [20] L. da F. Costa (2008), arXiv:0801.2520.
- [21] A. Arenas, A. Fernandez, and S. Gomez (2008), arXiv:physics/0703218.
- [22] R. Borisyuk, G. Borisyuk, and Y. Kazanovich, Behav. and Brain Sci. **21**, 833 (1998).
- [23] T. Aoki and T. Aoyagi (2004), arXiv:q-bio/0410029.
- [24] B. Percha, R. Dzakpasu, M. Zochowski, and J. Parent, Phys. Rev. E **72**, 031909 (2005).
- [25] P. Pereira, M. S. Baptista, and J. Kurths (2007), arXiv:0706.3317.
- [26] G. V. Osipov, J. Kurths, and C. Zhou, *Synchronization in Oscillatory Networks* (Springer, 2007).
- [27] H. Hasegawa, Phys. Rev. E **70**, 066107 (2004).
- [28] H. Hasegawa, Phys. Rev. E **72**, 056139 (2005).
- [29] S. M. Park and B. J. Kim, Phys. Rev. E **74**, 026114 (2006).
- [30] V. Latora and M. Baranger, Physical Review Letters **82**, 520 (1999).
- [31] J. G. Gardenes and V. Latora (2007), arXiv:0711.0278.
- [32] R. Albert and A. L. Barabási, Rev. Mod. Phys. **74**, 47 (2002).
- [33] M. E. J. Newman, SIAM Rev. **45**, 167 (2003).
- [34] S. N. Dorogovtsev and J. F. F. Mendes, Adv. in Phys. **51**, 1079 (2002).
- [35] L. da F. Costa, F. A. Rodrigues, G. Travieso, and P. R. V. Boas, Adv. in Phys. **56**, 167 (2007).
- [36] L. da F. Costa (2007), arXiv:0711.1271.
- [37] L. da F. Costa (2007), arXiv:0711.2736.
- [38] L. da F. Costa (2007), arXiv:0712.0415.
- [39] P. J. Flory, Journal of the American Chemical Society **63**, 3083 (1941).
- [40] L. da F. Costa, Phys. Rev. Lett. **93**, 098702 (2004).
- [41] L. da F. Costa, Phys. Rev. E **70**, 056106 (2004), cond-mat/0312712.
- [42] L. da F. Costa and R. F. S. Andrade, New J. Phys. **9**, 311 (2007).
- [43] L. da F. Costa and F. N. Silva, Journal of Statistical Physics **125**, 845 (2006).
- [44] L. da F. Costa and L. E. C. da Rocha, The Eur. Phys. J. B **50**, 237 (2005).
- [45] L. da F. Costa (2008), arXiv:0802.1272.
- [46] L. da F. Costa and R. M. Cesar, *Shape Analysis and Classification: Theory and Practice* (CRC Press, 2001).
- [47] G. J. McLachlan, *Discriminant Analysis and Statistical Pattern Recognition* (John Wiley and Sons, 1998).
- [48] R. O. Duda, P. E. Hart, and D. G. Stork, *Pattern Classification* (Wiley Interscience, 2000).
- [49] M. A. L. Nicolelis, *Methods for Neural Ensemble Recordings* (CRC Press, 1998).
- [50] L. da F. Costa (2008), arXiv:0802.0421.
- [51] L. da F. Costa (2008), arXiv:0801.3056.
- [52] L. da F. Costa (2008), arXiv:0801.4269.
- [53] L. da F. Costa (2008), arXiv:0801.4684.
- [54] L. da F. Costa, O. Sporns, L. Antigueira, M. G. V. Nunes, and O. N. Oliveira, Appl. Phys. Letts. **91**, 054107 (2007).
- [55] Though the order of the neurons in such diagrams is arbitrary, the way in which the WS networks were generated in this work tends to yield respective adjacency.
- [56] Interestingly, the activation dynamics in a complex neuronal network can be thought as involving random walks of moving agents, so that their movement can be tagged and tracked.



(a)



(b)

FIG. 11: The normalized instantaneous synchronizations at each node of the GG network considered in this article at times 100 (a) and 1000 (b).

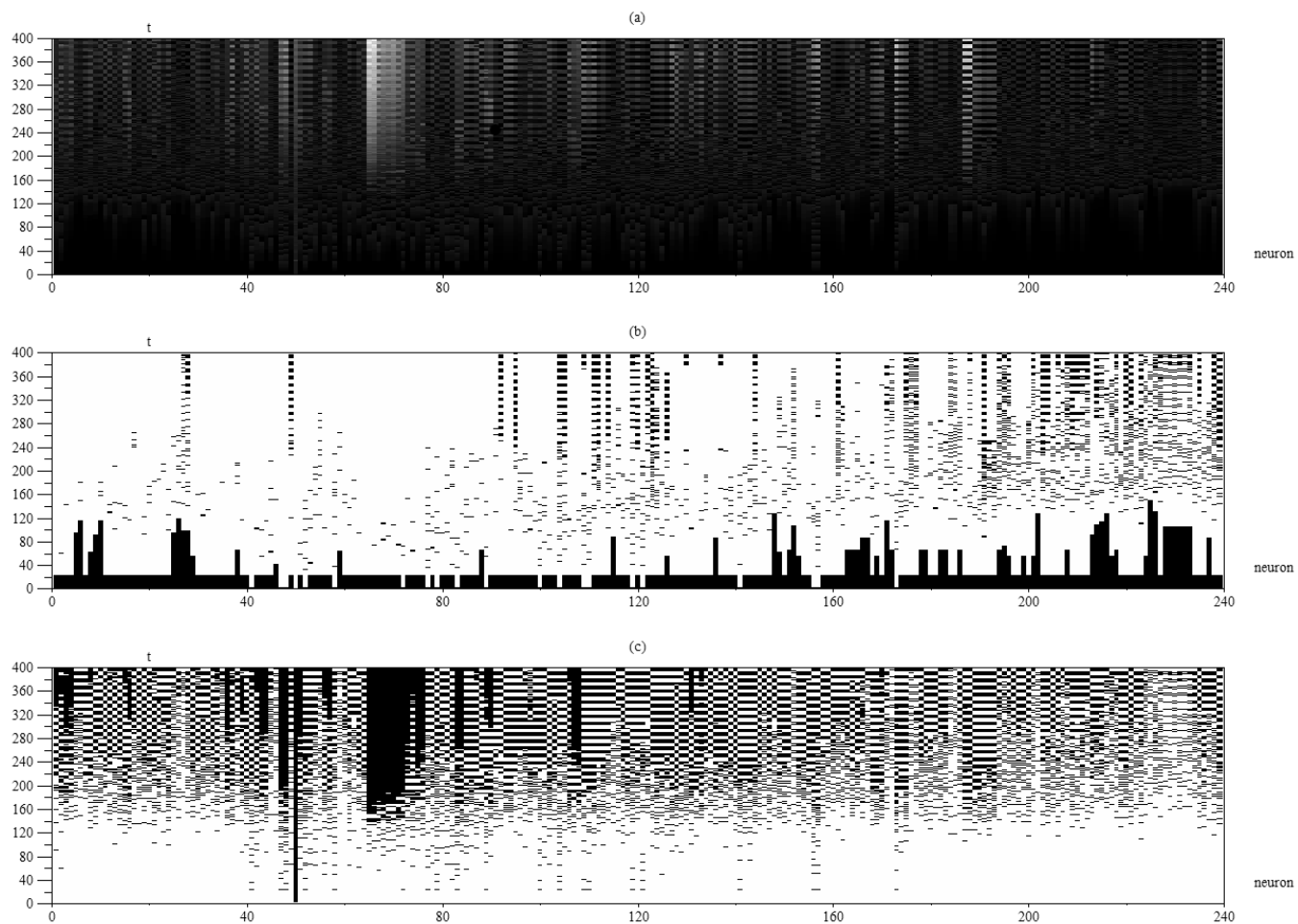


FIG. 12: The activation diagrams for the 239 nodes in the largest connected component of the *C. elegans* network.

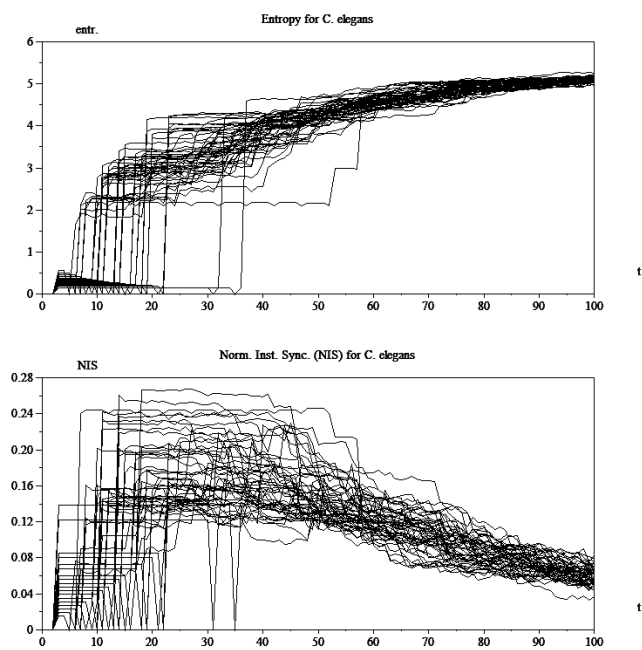


FIG. 13: The entropies and NISs along time for neurons 1 to 50 in the *C. elegans* network.

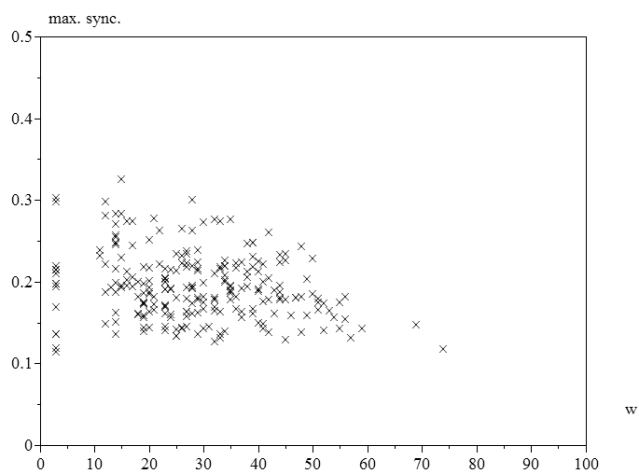


FIG. 14: The maximum NIS and respective times obtained along the initial 100 steps for the *C. elegans* network, considering the source placed at each of the nodes.

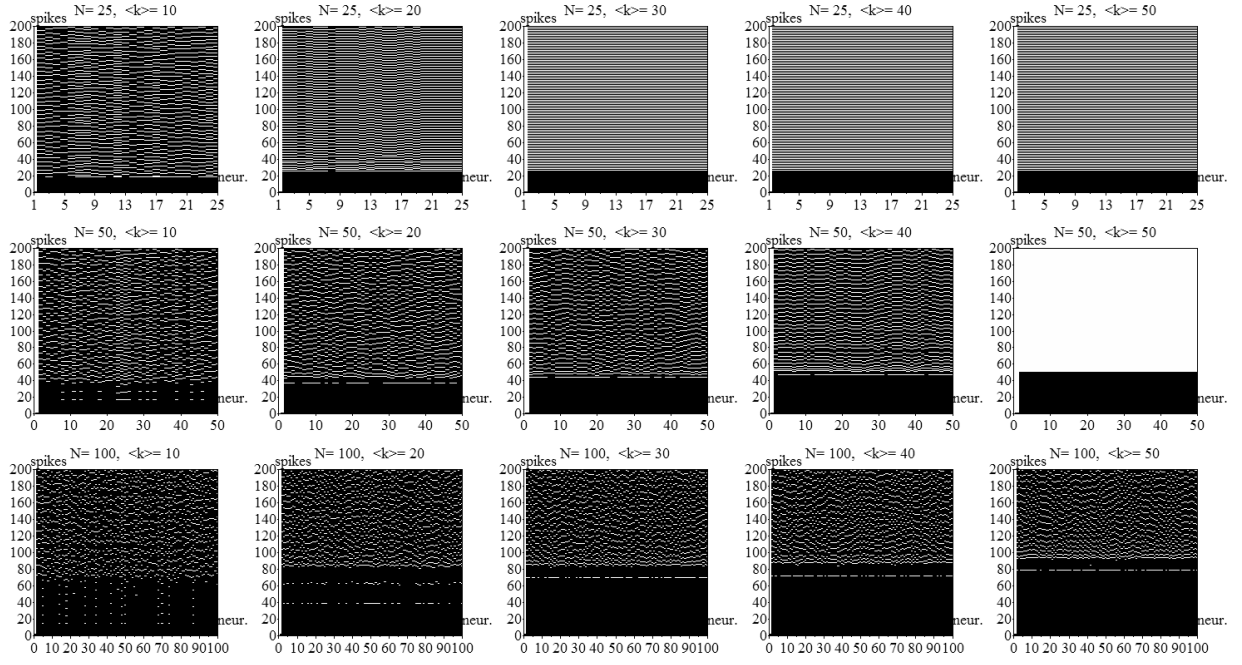


FIG. 15: The spikegrams, i.e. the occurrence of spikes for each neuron (identified along the x -axis) along time (y -axis) obtained for the ER configurations. Observe the avalanche transitions during the transient regime, as well as the increase of frequency regularity and synchronization with observed for larger values of average degree.

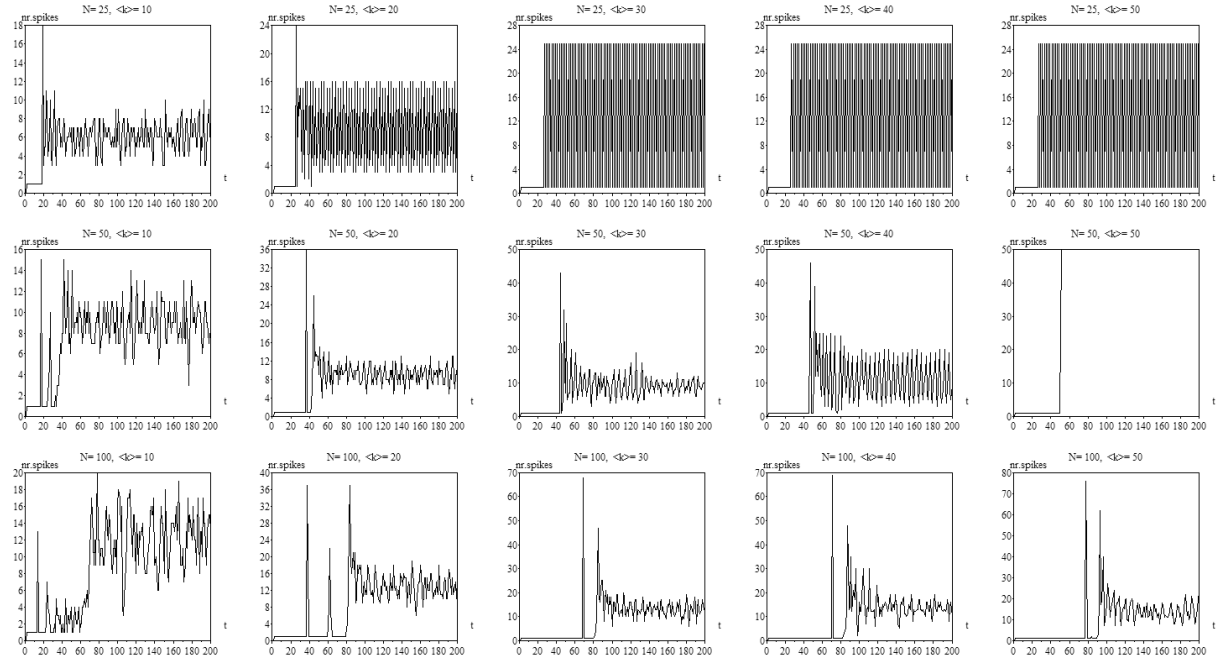


FIG. 16: The number of spikes along time obtained for the original ER complex network configurations.

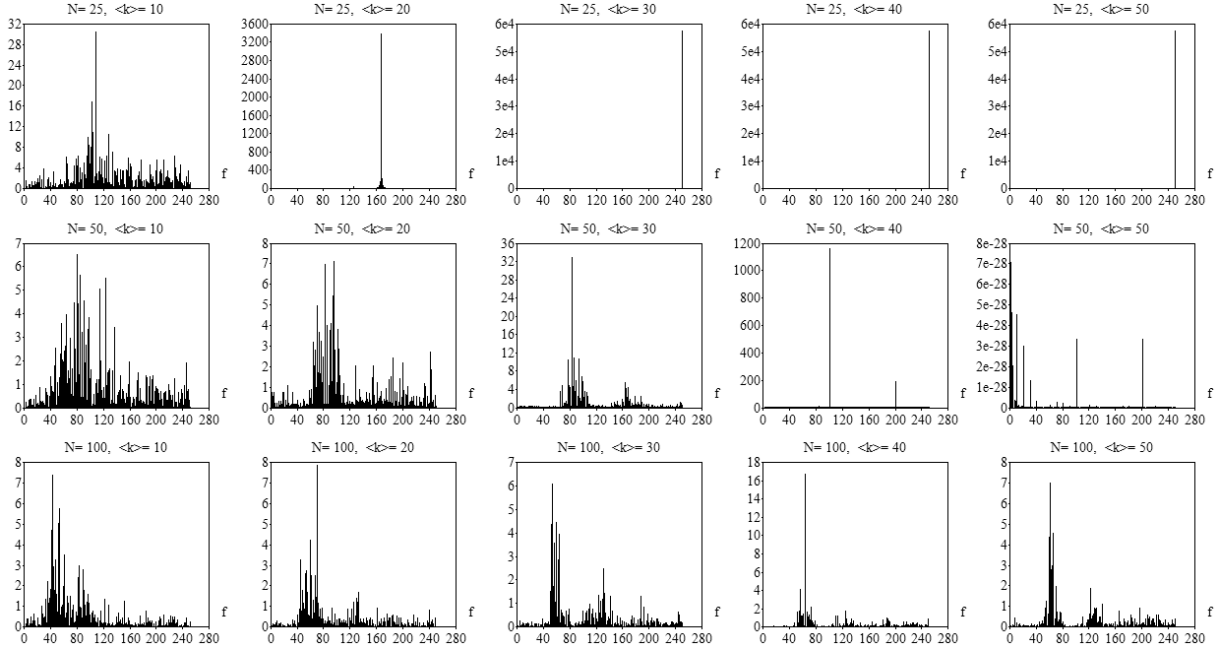


FIG. 17: The power spectra obtained for the number of spikes produced by the whole original ER networks.

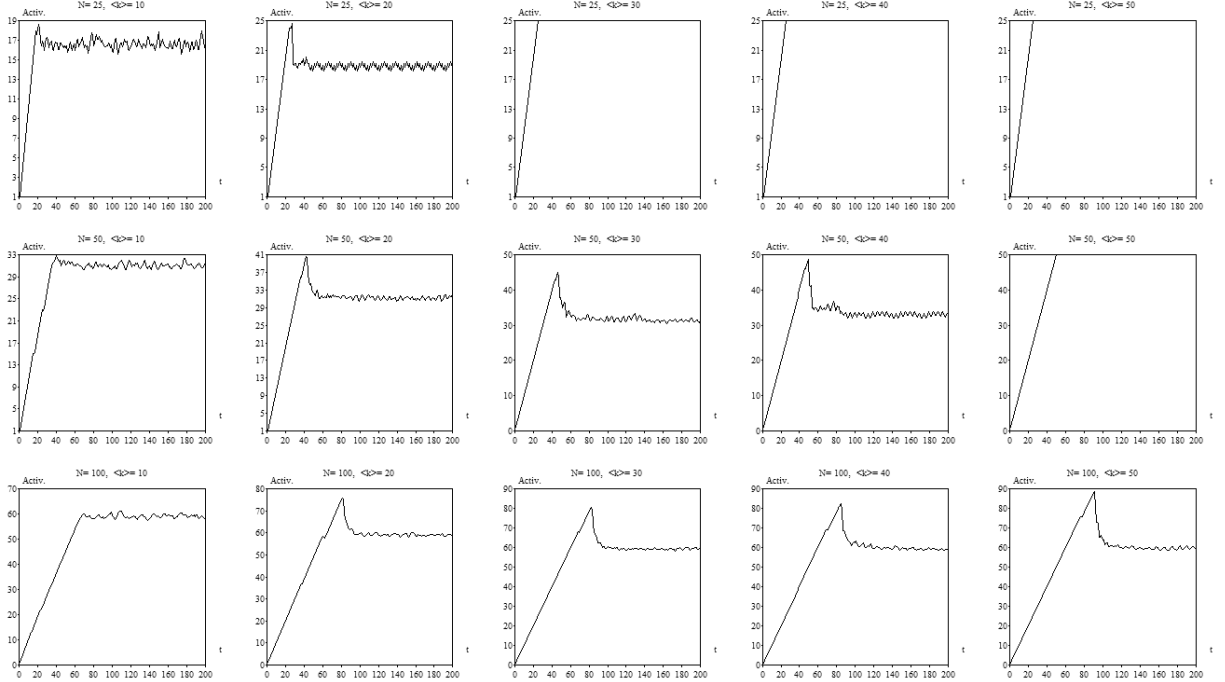


FIG. 18: The total activation inside the complex neuronal networks is not conserved (recall that activation is being continuously fed from the source node) after the main avalanche, but rather reaches a plateau of activation after the transient regime.

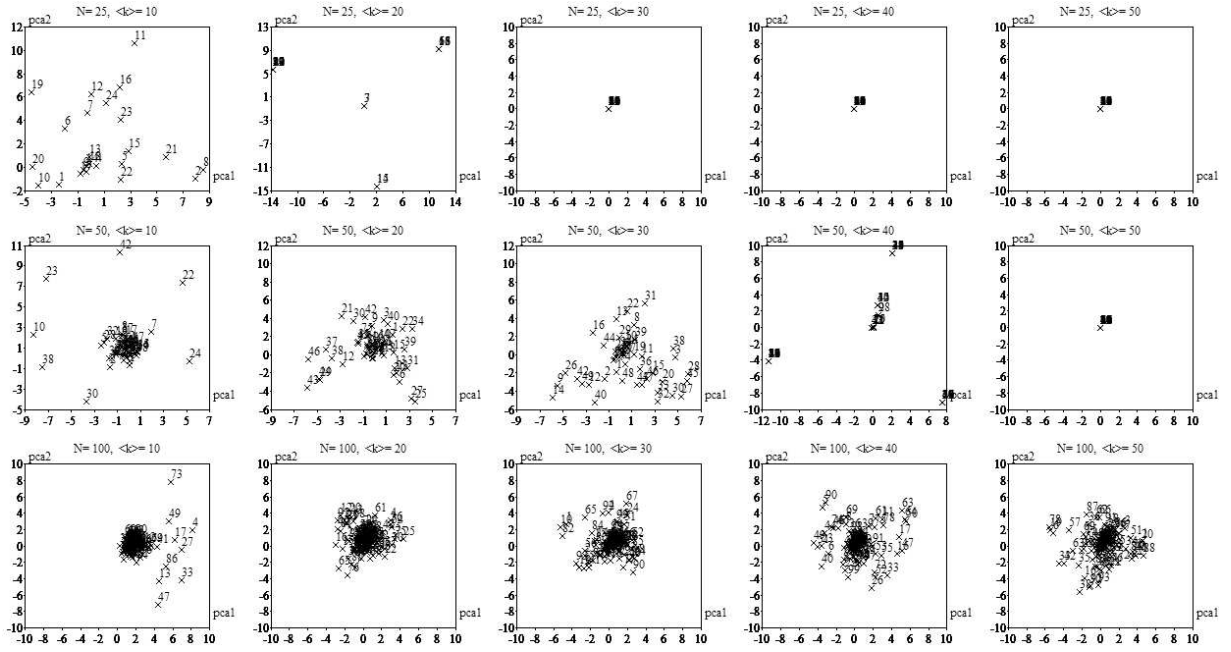


FIG. 19: The two-dimensional scatterplots obtained by the application of the PCA method over the spike patterns of each neuron in the ER configurations.

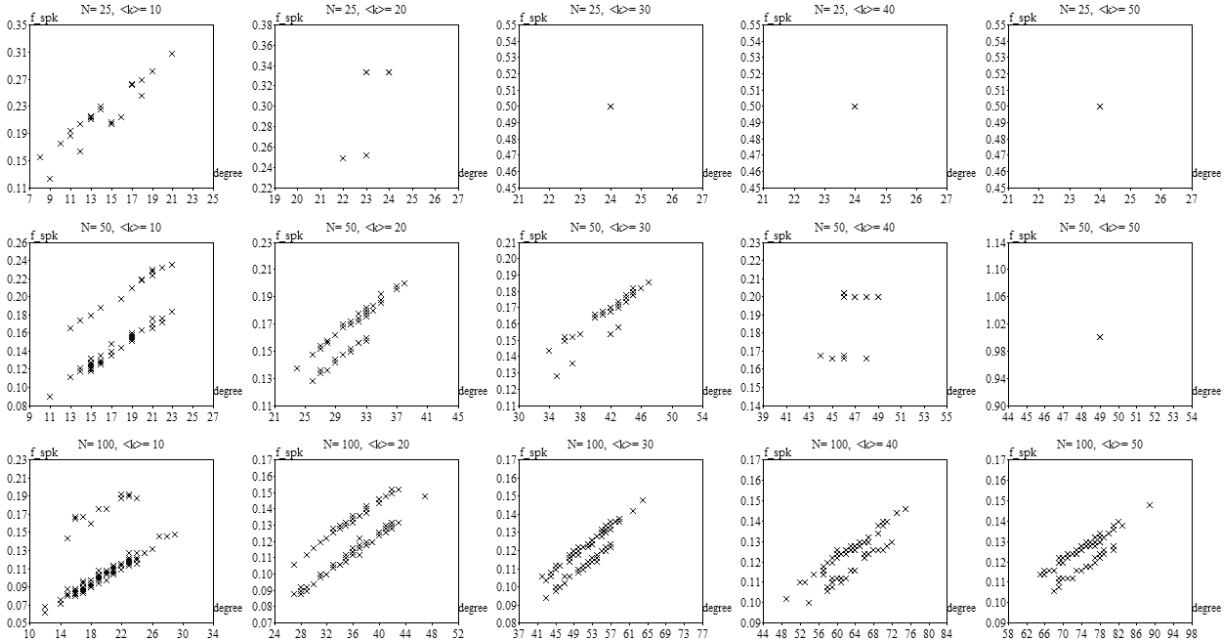


FIG. 20: The relationships between the total number of spikes per time step generated by each neuron and the respective degrees for all the considered ER configurations. The number of spikes were counted during the last 500 steps of 1000 steps-long signals.

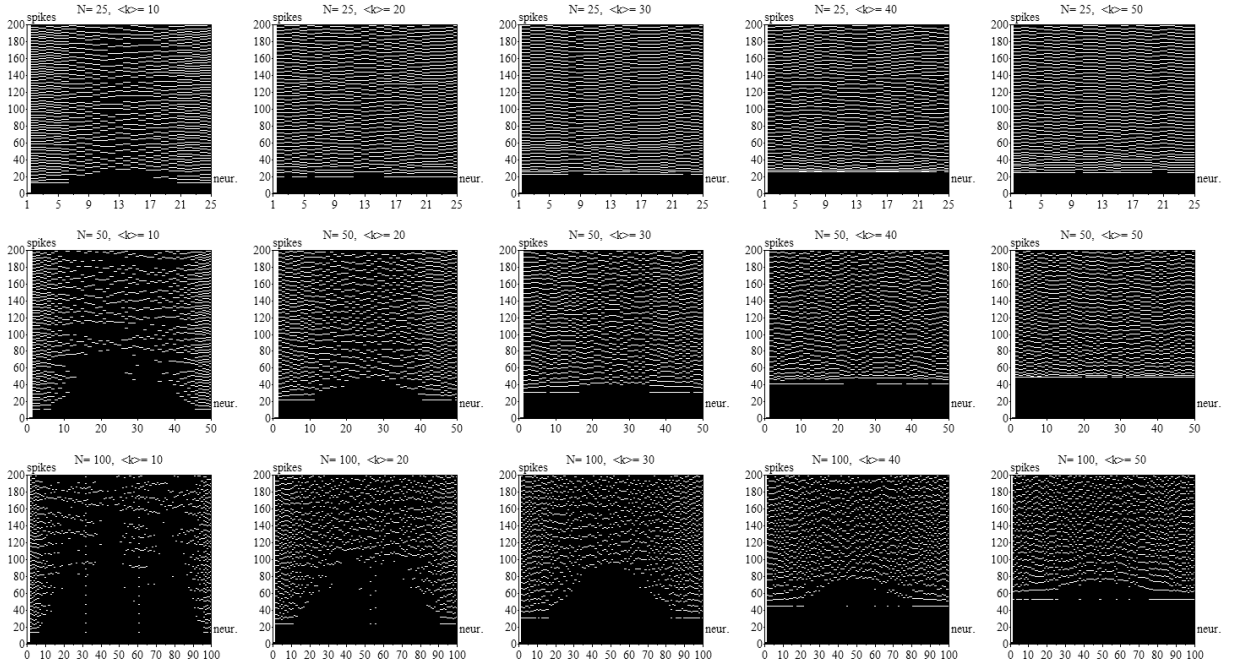


FIG. 21: The spikegrams obtained for the WS configurations.

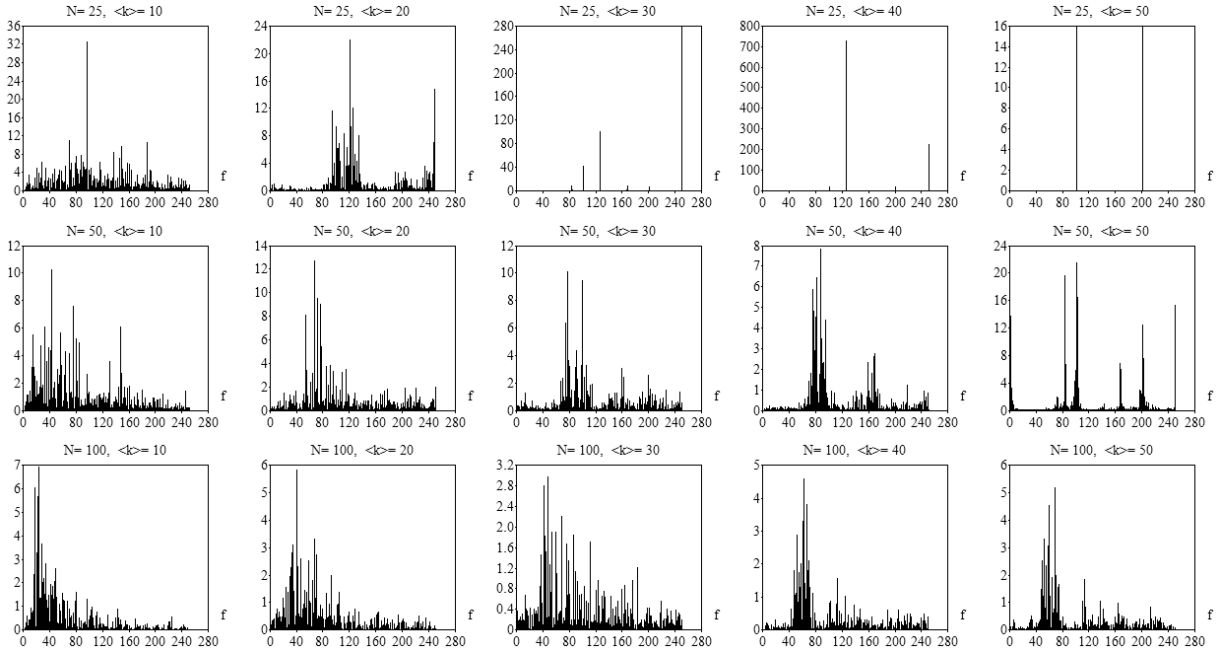


FIG. 22: The power spectra obtained for the number of spikes produced by the whole original WS networks.

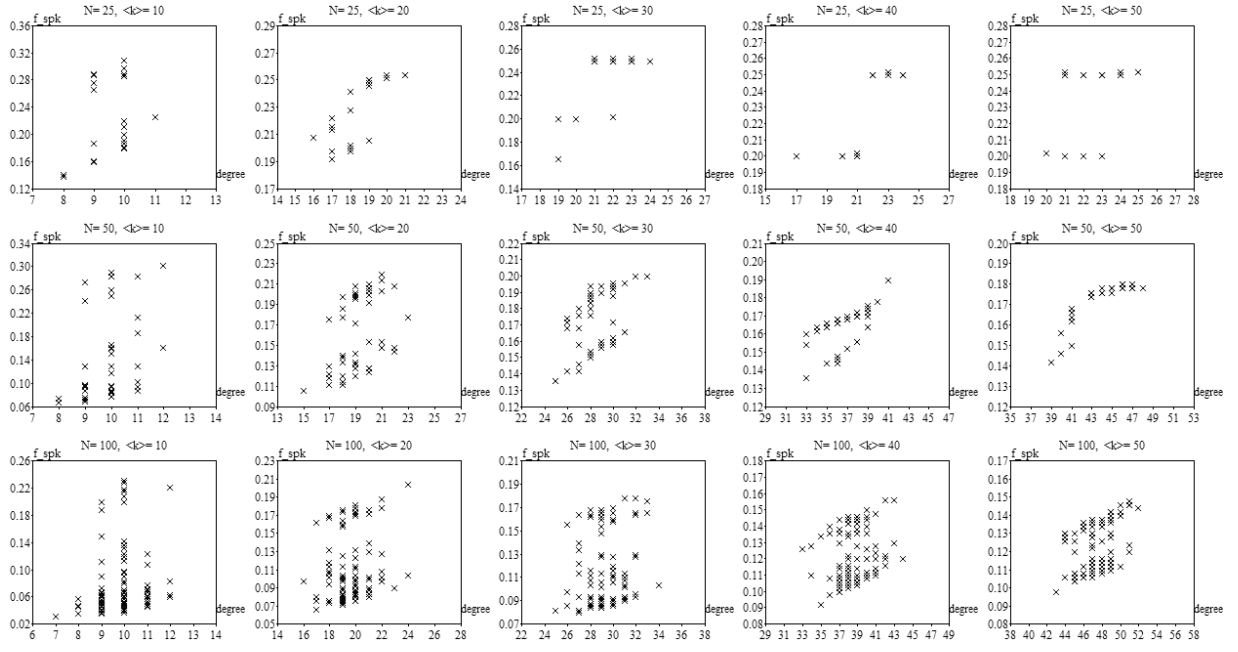


FIG. 23: The relationships between the total number of spikes per time step generated by each neuron and the respective degrees, all the considered WS configurations. The number of spikes were counted during 1000 time steps.

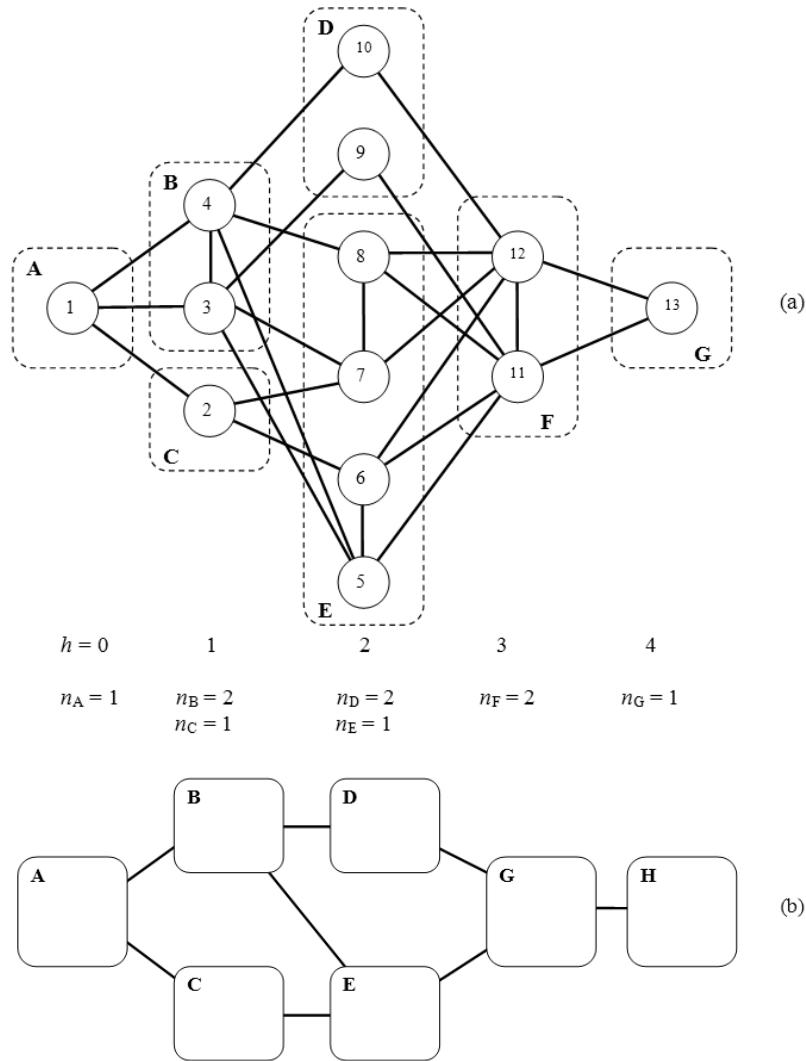


FIG. 24: The hierarchical organization of a simple network (a) with respect to node 1. A total of 5 concentric levels have been obtained. The dotted boxed identify the nodes with identical degrees at each concentric level, which are subsumed by the respective equivalent nodes, yielding the equivalent network shown in (b).

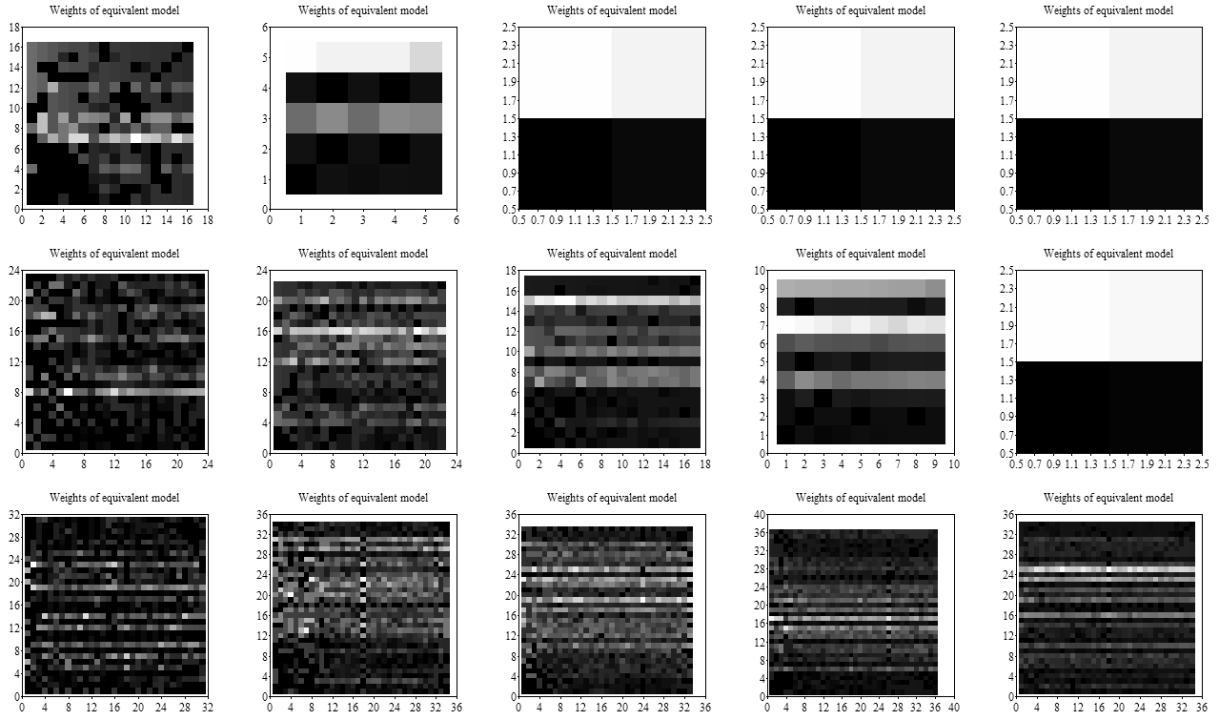


FIG. 25: The weights of each of the equivalent models obtained for the ER configurations.

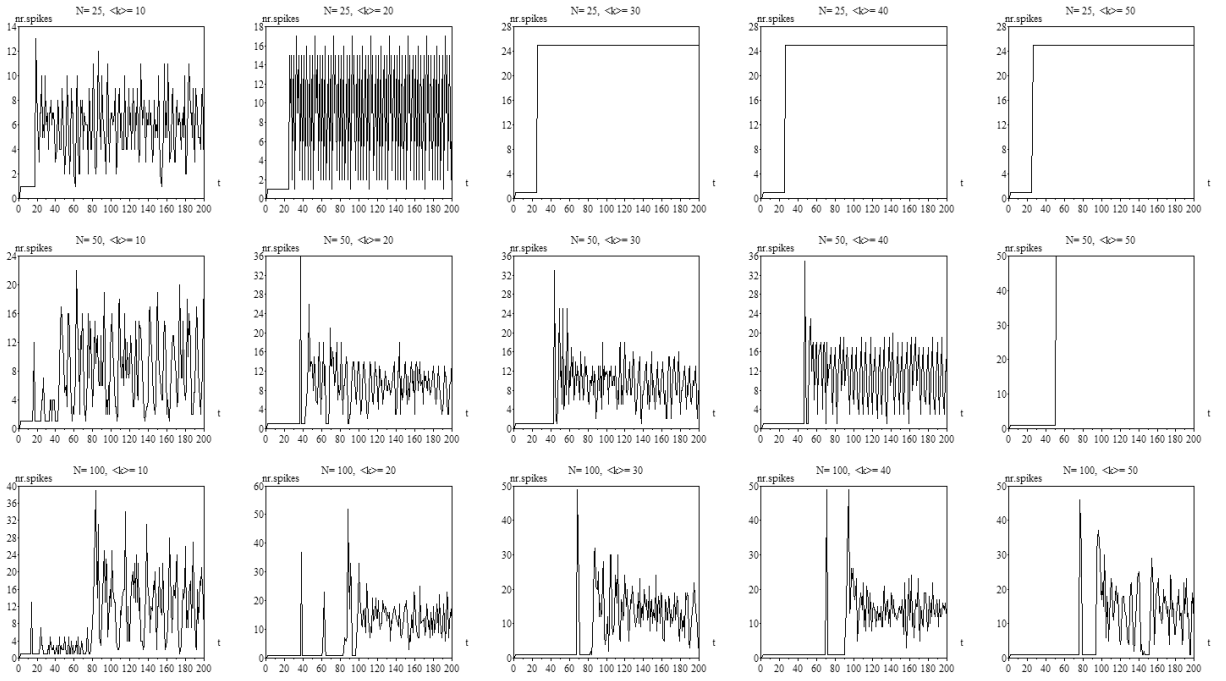


FIG. 26: The total number of spikes along time t for the ER configurations as predicted by the respective equivalent models.